Aus der

Berufsgenossenschaftlichen Unfallklinik

Klinik für Hand-, Plastische, Rekonstruktive und
Verbrennungschirurgie an der Universität Tübingen

Accelerating Skin Wound Healing in vitro - Establishment of an External Electrical Field System for Stimulating Keratinocytes

Inaugural-Dissertation
zur Erlangung des Doktorgrades
der Medizin

der Medizinischen Fakultät
der Eberhard Karls Universität
zu Tübingen

vorgelegt von

Lu, Chao

2022

Dekan: Professor Dr. B. Pichler

1. Berichterstatter Privatdozent Dr. J. Kolbenschlag
2. Berichterstatter: Professor Dr. H.-M. Häfner

Tag der Disputation: 10.11.2022

Table of Contents

List of abbreviations

bFGF	Basic fibroblast growth factor
DMEM	Dulbecco's modified eagle medium
DNA	Deoxyribonucleic acid
DPBS	Dulbecco's Phosphate Buffered Saline
ECM	Excessive extracellular matrix
ECL	Enhanced chemiluminescence
EF	Electrical field
EFs	Electrical fields
EMFs	Electromagnetic fields
ES	Electrical stimulation
FGF-7	Fibroblast growth factor-7
GAPDH	Glyceraldehyde 3-phosphate dehydrogenase
GM-CSF	Granulocyte-macrophage colony-stimulating factor
HRP	Horseradish peroxidase
MAPK	Mitogen-activated protein kinase
MMPs	Matrix metalloproteinases
PDGF-AB	Platelet-derived growth factor AB
RT	Room Temperature
SRB	Sulforhodamine B
TBS-T	Tris-buffered saline/Tween 20
TEP	Transepithelial potential

1. Introduction

1.1. Skin and wound healing

1.1.1. Skin function and structure

As the largest organ of the human body, the total weight of skin is about 16% of the adult's body weight, and it has a surface area of about 2 m^2 and thickness of about 0.5-4.0 mm (Chamcheu *et al.*, 2019). Human skin acts as a physiological and physical barrier that shields internal tissues from the harmful external environment (Rodrigues *et al.*, 2019). It has different functions in protecting the body from mechanical damage, microbial infection, ultraviolet radiation, and excessive moisture transpiration (Fore, 2006) (Figure 1.1.).

The skin consists of epidermis, dermis, and subcutaneous tissue. As the outermost layer of the skin, the epidermis prevents pathogens from entering and transcutaneous water loss (Grainger, 2014). In the human epidermis, up to 95% of cells are keratinocytes, and the remaining 5% are Merkel cells, melanocytes, and Langerhans cells (Quaresma, 2019). Keratinocytes, the major cells in the epidermis, are responsible for repairing the integrity of the skin after injury via epithelialization (Bucekova *et al.*, 2017). The proliferation and migration ability of keratinocytes is critical in the wound healing process; thus, keratinocytes are frequently used as a model of *in vitro* wound healing research (Mahmoud *et al.*, 2019). For instance, the immortalized nontumorigenic human epidermal (HaCaT) cells are ideal and widely used candidates for *in vitro* skin wound healing investigations (Schoop *et al.*, 1999).

The dermis layer of skin is beneath the epidermis. Through a basal membrane, it is tightly connected to the epidermis. It harbors connective tissues, blood vessels, lymphatics, nerves endings, and the various skin appendages (hair follicles, sebaceous glands, sweat glands, *etc.*) (Xia *et al.*, 2020). The presence of collagen, elastin, fibrillin, and glycoproteins in the dermis layer allows the skin to gain the properties of suppleness and mechanical strength (Chamcheu *et al.*, 2011, Labat-Robert, 2012, Quan and Fisher, 2015), thus cushioning the body from stress and strain.

Underneath the dermis lies the subcutaneous tissue. It is the deepest skin layer, which lies closest to the muscle, and consists primarily of loose connective tissue and blood vessels, which protect the body and keep it warm (Gilaberte *et al.*, 2016). Besides, fat tissue in the subcutaneous layer has been generally regarded as an excellent energy reservoir (Kwon *et al.*, 2017).

Human skin provides a crucial barrier against hazardous environmental factors (foreign particles, chemicals, pathogens, ultraviolet rays, *etc*.) (Kalailingam *et al.*, 2019). Thus, skin health and integrity are vital for humans. However, skin injury is an inevitable event of everyday human life, making wound healing an essential process for maintaining good health and well-being.

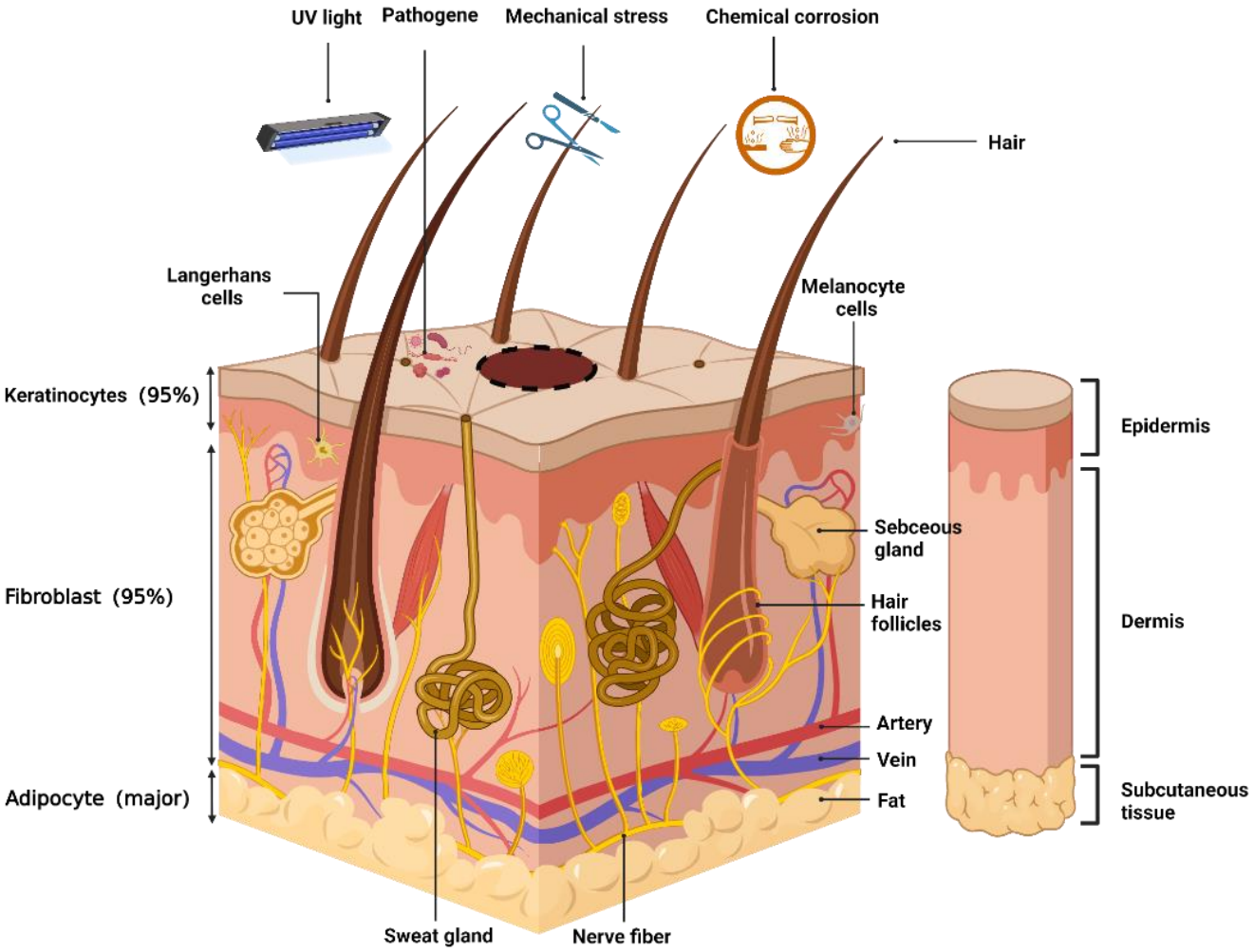

Figure 1.1. Schematic representation of skin structure. The skin consists of three layers. The outermost stratum, the epidermis, predominantly consists of keratinocytes; it is responsible for preventing pathogens from entering the body and transcutaneous water loss. The dermis is a collagen-rich and thick stratum of skin; the presence of collagen, elastin, fibrillin, and glycoproteins in the dermis layer allows the skin to gain the properties of suppleness and mechanical strength. The subcutaneous tissue stratum is the deepest skin layer, consisting primarily of loose connective tissue and blood vessels, thus protecting the body and keeping it warm. Inspired by (Nikitkina *et al.*, 2021). *Created with BioRender.com*

1.1.2. Wound healing is a dynamic, ordered, and highly orchestrated process.

Wound healing proceeds in three temporal sequences with overlapping phases: hemostasis/inflammation, re-epithelialization, and tissue remodeling (Gurtner *et al.*, 2008) (Figure 1.2.). Immediately after tissue damage, hemostasis and inflammation are triggered. The coagulation cascade, inflammatory pathways, and immune system perform vital functions to seal and clean up the wound site (Wonga and Maha, 2021). This phase continues from 2 hours to 2 weeks (Gonzalez *et al.*, 2016) (Figure 1.2.A).

The second phase of wound healing, re-epithelialization, is characterized by the proliferation and migration of different cell types (keratinocytes, fibroblasts, *etc.*) (Won *et al.*, 2019). In this stage, sprouts of new blood vessels (also known as angiogenesis) provide the necessary substances to the wound site and intermingle with the provisional matrix composed mainly of a fibrin mix (Aller *et al.*, 2010). The arrival of new capillaries associated with fibroblast and macrophages converts fibrin into granulation tissue (Eming *et al.*, 2007), which repopulates the wounded area and provides a scaffold for keratinocyte proliferation and migration, thus restoring the barrier function of the epithelium (Aller *et al.*, 2010, Tonnesen *et al.*, 2000). As a critical event of this stage, angiogenesis is managed by a series of cytokines and growth factors (*e.g.*, vascular endothelial growth factor [VEGF], granulocyte-macrophage colony-stimulating factor [GM-CSF], *etc.*). It is a critical process in the rate and quality of wound healing both *in vivo* and *in vitro* (Blache and Ehrbar, 2018). The re-epithelialization stage occurs 2-10 days after injury (Won *et al.*, 2019). At this stage, parts of fibroblasts differentiate into myofibroblasts (contractile cells) under the stimuli of macrophages, mediating wound contraction to bring wound margins together (Seo and Jung, 2016), and secretion of the extracellular matrix (ECM) mainly in the form of collagen, which is a component of scar tissue (Figure 1.2.B).

Remodeling is the third and most extensive phase of healing, which begins approximately 2 weeks after injury and lasts for over a year (Gurtner *et al.*, 2008), including maturation and remodeling of the new tissue (Schäfer and Werner, 2008). At this stage, the events activated by injury in the wound site gradually

wind down and cease. As programmed cell death commences, endothelial cells, most of the myofibroblasts, and macrophages undergo apoptosis or exit from the wound site (Szabowski *et al.*, 2000). Meanwhile, residual cells, as described above, start to secrete matrix metalloproteinases (MMPs), which act on a variety of ECM substrates, and predominantly remodel type III collagen that is synthesized during the re-epithelialization stage into more vital type I collagen (Henriksen *et al.*, 2020). As a result, the scar size is reduced and the tensile strength is increased (Soib *et al.*, 2020). Thus, a mature and stable scar is formed, marking the end of wound healing (Figure 1.2. C).

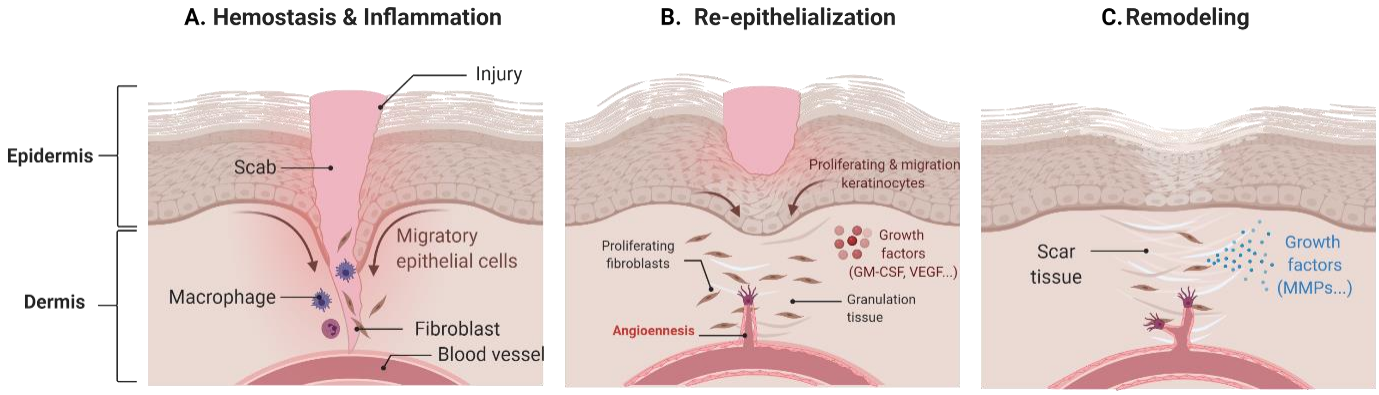

Figure 1.2. Schematic illustration of the wound healing process. Wound healing proceeds in three overlapping phases. (A) The hemostasis and inflammation phase occur immediately following skin injury. The wound is sealed by a clot in a short time, inflammatory cells are recruited to the wound site. (B. The re-epithelialization phase is characterized by the proliferation and migration of different cell types, meanwhile, the secretion of ECM by fibroblasts fosters the formation of granulation tissue, which contributes to the angiogenesis progress. (C) The remodeling phase is the last and the most extended phase of healing. Cells at the wound site secrete MMPs, which can remodel type III collagen into more vital type I collagen, leading to an increase in the tensile strength of the wound. Inspired by (Cancedda *et al.*, 2017). *Created with BioRender.com*

1.2. Transepithelial potential difference (TEP) was identified as one of the key signals to initiate the process of wound healing

1.2.1. The generation of the TEP

Transepithelial ion transport and the isolative character of the epithelium play central roles in the generation of the TEP. On the membranes of skin cells, ion channels and pumps transport cations (mainly sodium) inwards to the basal side and chlorine ions out to the apical side, thus establishing a potential difference on opposite sides of the epithelium of the skin (Levin and Verkman, 2005, Levin *et al.*, 2006). Meanwhile, cells in this layer are connected by tight and resistive junctions, forming an insulating barrier, maintaining this TEP. Researchers have made attempts to investigate this transmembrane voltage drop by placing reference electrodes underneath and on the top of skin (Barker *et al.*, 1982), and they reported the voltage of the TEP ranging from 10 mV to 60 mV (approximately 200 mV/mm), depending on the area of human skin measured (Foulds and Barker, 1983). TEPs are also present in almost all types of epithelia in the human body (Zhao, 2009), and the principles are similar to those described in the epithelium of the skin. New findings have suggested that TEPs play an overriding role in guiding the biological behaviors of cells (*e.g.*; migration, differentiation, *etc.*) (McCaig *et al.*, 2005, Levin, 2007). Furthermore, researchers have realized that the TEP might be a key signal for triggering the growth of the central nervous system (Shapiro *et al.*, 2005), tumorigenesis (Kirson *et al.*, 2004), and in particular, wound healing (Rajnicek *et al.*, 1988).

1.2.2. TEP and wound healing

Endogenous electrical fields at human wound sites were detected over 150 years ago by the German physiologist Emile Du Bois Reymond (McCaig, 2008). Since then, researchers have started to consider whether this electrical signal has an effect on wound healing, and growing evidence has shown that the existence of

endogenous electrical fields, or put differently, the TEP is crucial for all stages of the physiological process of wound healing (Luo *et al.*, 2021b). More interestingly, for wounds that do not heal spontaneously, an applied electrical stimulation (ES) can improve the outcome of treatment (Strecker-McGraw *et al.*, 2007).

The TEP involves exercising several functions in different phases of the wound healing process (Figure 1.3.). In the inflammation phase of wound healing, the variation in endogenous electrical fields can recruit immunocytes (*e.g.*, macrophages, lymphocytes, neutrophils, *etc.*) to the wound site (Tandon *et al.*, 2009). This is mainly due to the voltage-gated potassium channels of the immunocytes, which can be mediated by EFs (electric fields) signals (Franklin *et al.*, 2016), and in turn, change the electrotaxis of immune cells. In this phase, the recruitment of immunocytes (macrophages, neutrophils, *etc.*) is beneficial to clear the pathogen and foreign bodies, thus reducing the risk of infection and priming for the next step of wound repair (Yaron *et al.*, 2020).

During the re-epithelialization phase, the main contribution of the local TEP changes to wound healing is reflected in accelerating the blood flow of tissue (Wolcott *et al.*, 1969, Kemppainen *et al.*, 1994) and promoting the migration and proliferation of cells such as epithelial and endothelial cells (Foulds and Barker, 1983, Harrison-Balestra *et al.*, 2003, Nishimura *et al.*, 1996, Zhao *et al.*, 2004, Hang *et al.*, 1995). Accumulating evidence has indicated that, with exposure to exogenous EFs, the increase in blood flow contributes to the delivery of nutrients (Wolcott *et al.*, 1969, Kemppainen *et al.*, 1994) and the regression of edema (Edwick *et al.*, 2022). Meanwhile, the EF-mediated migration of keratinocytes (Jaffe and Vanable Jr, 1984, Nishimura *et al.*, 1996), the proliferation of fibroblasts (Dunn *et al.*, 1988), and migration of endothelial cells (angiogenesis) (Zhao *et al.*, 2004, Hang *et al.*, 1995) cause the acceleration of the re-epithelialization process, playing an indispensable role in this stage.

In the third phase of wound healing, the remodeling phase, collagen is deposited; thus, scar tissue is formed. Excessive scarring is an abnormal fibroproliferative process, resulting in hypertrophic scarring and keloid formation (Walmsley *et al.*, 2015). Excessive scarring may result in a crab claw-like appearance, pain, pruritis, and skin irritation around the wound site (Schmitz *et al.*, 2019). Accumulating

evidence has indicated that ES can also be significant in the formation of scar tissue, or other words, the remodeling phase of wound healing. For instance, in the study by Weiss *et al.*, skin scars' thickness was first discovered to be related to exposure to exogenous EFs (Weiss *et al.*, 1989). Similarly, Ambic *et al.* found that ES had a particular effect on the hardness of scars (Ambic *et al.*, 1993). Although the mechanism behind it was not elucidated, some studies pointed out that it might be due to the effects of EFs on collagen deposition (Thawer and Houghton, 2001).

Collectively, *in vivo* experiments confirmed the promising potential effects of EFs on different stages of wound healing. Despite their molecular and genetic mechanisms not being very clear, the roles of EFs in the diverse responses of different times, spaces, and cell types of wound healing are crucial in understanding the mysteries of wound healing.

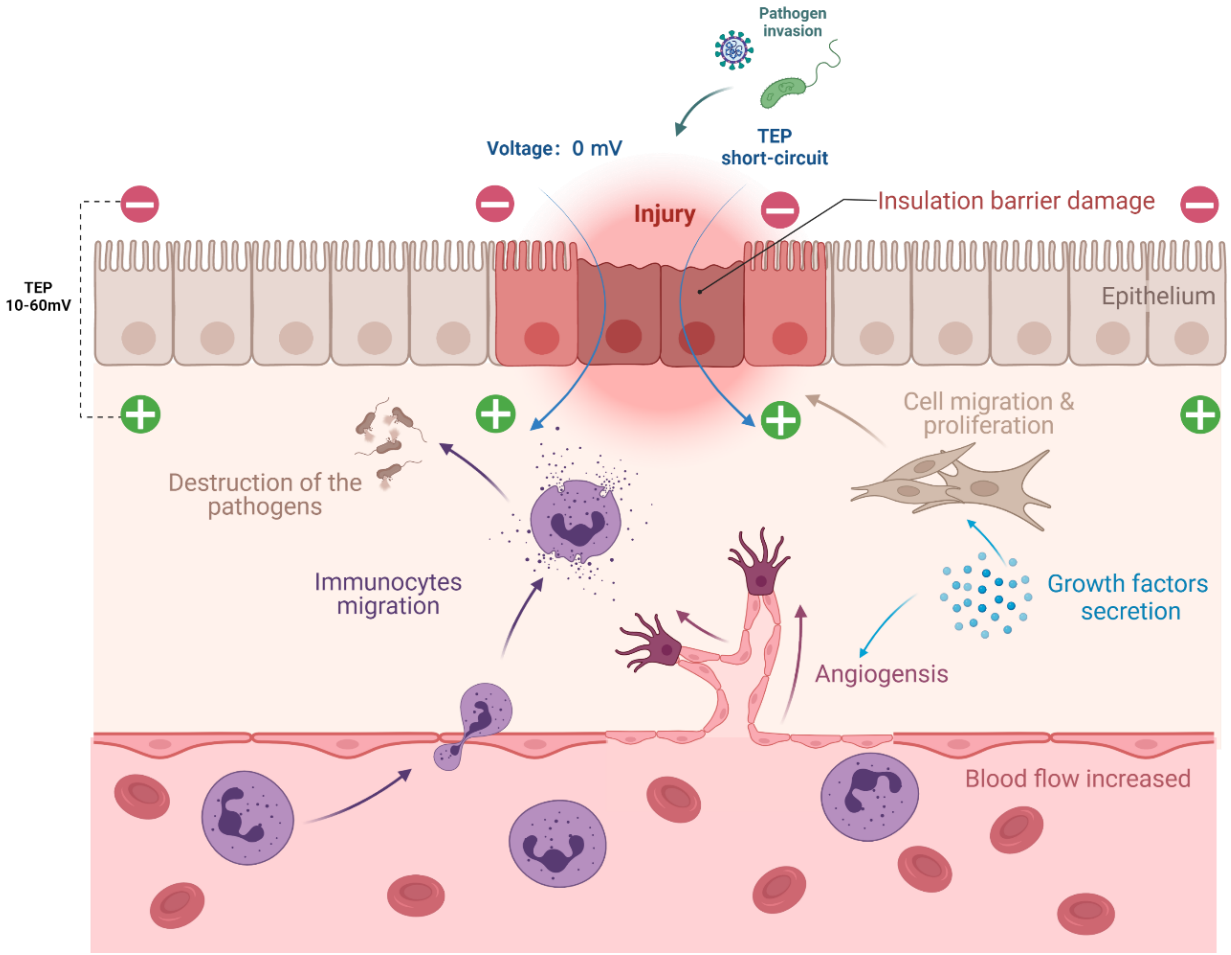

Figure 1.3. Transepithelial potential (TEP) and the endogenous EFs of skin wounds are essential in initiating and regulating wound healing. Immediately after tissue injury, TEP was generated. TEP recruits immunocytes (*e.g.*, macrophages, lymphocytes, neutrophils, *etc.*) to the wound site in the inflammation phase, thus reducing the risk of infection. TEP-mediated migration of keratinocytes and endothelial cells causes the acceleration of the re-epithelialization process. It increases blood flow, thus contributing to the delivery of nutrients and the regression of edema. Inspired from (Zhao, 2009). *Created with BioRender.com*

1.2.3. Status and difficulty of *in vitro* EF stimulation research

The clinical application of EFs to improve wound healing outcomes is well developed (Ud-Din and Bayat, 2014). Interestingly, the *in vitro* research on exogenous ES treatment is less optimistic compared to its enormous success

clinically (Polak *et al.*, 2017, Polak *et al.*, 2016, Ahmad, 2008). The crucial constraint in achieving *in vitro* EF stimulation research is transmitting electrical signals to a cell culture system. The mainstream methods of delivering the stimulus are direct coupling stimulation, capacitive stimulation, and electromagnetic stimulation. However, each method has its strengths and weaknesses, and non-unified methods have led to diverging study results (Balint *et al.*, 2013).

A. Direct coupling stimulation

Direct Coupling Stimulation (Fig 1.4.A) is the simplest way of delivering electrical signals. With direct coupling, the electrodes or alternative electrodes are in direct contact with the cell culture medium, enabling efficient and fast transmission of electrical signals (Kim *et al.*, 2009, Ercan and Webster, 2010, Merrill *et al.*, 2005, Lu *et al.*, 2021). Although this is the most cost-effective and convenient method to investigate the effect of EFs *in vitro*, there are quite a few notable shortcomings. First, while delivering the EF signals, the pH value of the culture medium can be changed significantly due to the insufficient biocompatibility of the electrodes. Second, reduction-oxidation (redox) reactions inevitably occur at the conventional metal electrodes and the culture medium; thus, a considerable amount of reactive oxygen species is liberated (Björninen *et al.*, 2017, Ercan and Webster, 2010, Merrill *et al.*, 2005, Spadaro and Becker, 1979), which can interfere with the normal metabolism of cells. Last but not least, as the duration of the experiment increases, the electrical current will gradually heat the medium, making the temperature increase and inevitably disturbing the experiment (Song *et al.*, 2007).

B. Capacitive coupling stimulation

The capacitive coupling stimulation (Fig 1.4.B) setup comprises two capacitive plates connected with the power source. Due to the presence of a potential difference, a homogenous EF signal is created between two metal or carbon capacitive plates. Cells or tissues cultured in the medium can be put in the gap of the plates, thus receiving the ES (Au *et al.*, 2007, Kim *et al.*, 2009, Sauer *et al.*, 2005, Ercan and Webster, 2010). The advantages of this structure are: ***a.*** generation of reactive oxygen species and alternations of pH value are avoided

by the non-contact electrodes and ***b.*** the non-contact electrodes allow uniform EF stimulation to a population of cells, regardless of the position in the culture plate. However, the following shortcomings are apparent: ***a.*** a high voltage (Balint *et al.*, 2013) is required between the capacitive plates (*e.g.*, 1000 V between the capacitors can only generate an EF with a strength of 3.0 mV/mm) (Lu *et al.*, 2021), hence decreasing the security of the experiments and ***b.*** the gap between the capacitive plates has to be restricted to a small range (*e.g.*, 0.5-2.0 mm) to yield an adequately strong EF signal (Zamora-Navas *et al.*, 1995), which means that tailor-made cell culture vessels are required.

C. Electromagnetic stimulation

Electromagnetic stimulation (Fig 1.4.C) devices generate electromagnetic fields by coils placed under or around the cell culture vessels, thereby stimulating cells or tissues (Titushkin and Cho, 2009, Chen *et al.*, 2021). As another way of direct coupling stimulation, the advantages of this method are similar to capacitive coupling stimulation; however, such a scheme has specific limits, such as ***a.*** induced EFs are generated by alternating magnetic fields; therefore, the biological and molecular effects of the experimental subject are not caused by a single variable and ***b.*** electromagnetic field generators are generally expensive, thereby limiting access.

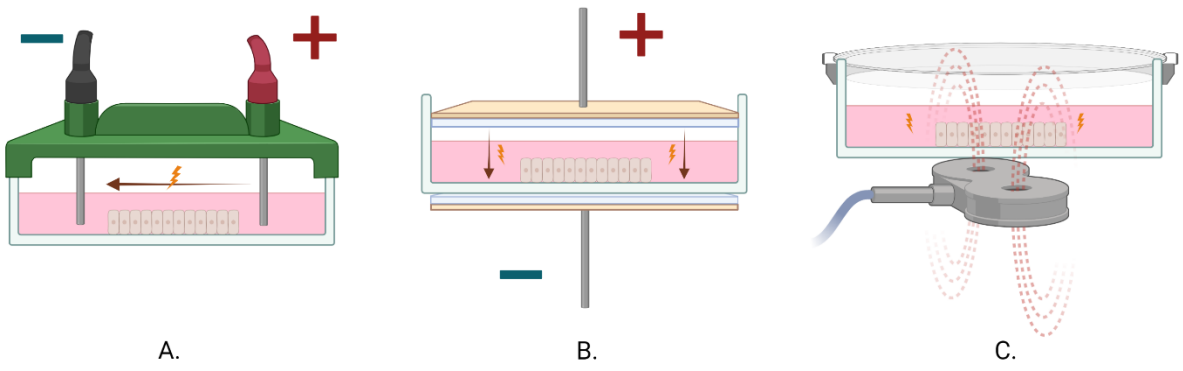

Fig 1.4. Three mainstream methods of delivering the stimulus. A.) direct coupling stimulation. B.) capacitive coupling stimulation. C.) electromagnetic stimulation. Inspired by (Balint *et al.*, 2013). *Created with BioRender.com*

1.3. Aim of the study

This study was designed to establish a practical ES system based on the principles of direct coupling stimulation, which addresses the limitations of replication mentioned in section 1.2.3. Using the newly designed ES system, we aimed to investigate the effects of EFs on the skin wound healing process (*e.g.*, cell migration, proliferation, growth factor secretion, *etc.*) *in vitro* (Lu *et al.*, 2021). Specifically, the following objectives were addressed in this study:

1. The establishment of an ES system and its characterization.
2. Test the migration ability after EF exposure.
3. Test the cell proliferation after EF exposure.
4. Measure the secretion of healing-associated cytokines that might be modified by EFs.
5. Investigate the potential molecular targets of EFs in HaCaT cells.

2. Materials and Methods

2.1. Materials

A comprehensive list of chemicals and reagents used in this study is provided in Table 2.1.

2.1.1. Chemicals and reagents

Table 2.1: List of used chemicals and reagents.

Substance	Article No.	Company
Acetic Acid Glacial (100%)	20104.298	VWR
1,9-Dimethyl-Methylene Blue Zinc Chloride Double Salt (DMMB)	341088	Sigma
Agarose	2267.4	Roth
Antibiotic/Antimycotic Stock Solution	P11-002	PAA
Boric Acid 99.8% p.a	6943.1	Carl Roth
Calcein Acetoxymethyl Easter (Calcein AM)	ABD-22002	ATT Bioquest
Chloroform	Y015.1	Carl Roth
Collagenase II	17454.01	Serva
Deoxyribonucleic Acid from Calf Thymus	D4522	Sigma
Diethylpyrocarbonate (DEPC)	K028.3	Carl Roth
Dimethyl Sulfoxide (DMSO)	4720.2	Carl Roth
Disodium Hydrogen Phosphate	7876.7	Carl Roth
Dulbecco's Phosphate Buffered Saline (DPBS)	D8537	Sigma
Ethanol 99.9% p.a. (EtOH)	20821.33	VWR
Ethidium Bromide 1%	2218.1	Carl Roth
Fetal Calf Serum (FCS)	41G7141K	Invitrogen
First Strand cDNA Synthesis Kit	K1621	ThermoFisher
Formaldehyde, 37% solution	A0823.1000	AppliChem
Glycerol, >99% p.a.	G6376-100G	Sigma

Glycine	3908.2	Carl Roth
Glycine, >99%, p.a.	A1067.5000	AppliChem
Guanidine Hydrochloride	G3272	Sigma
Guanidine Thiocyanate	0017.1	Carl Roth
Hoechst 33342	14533-100MG	Sigma
RayBio Human Growth Factor Array	AAH-GF-1-2	RayBiotech
Hyaluronic Acid Sodium	53747	Sigma
Hydrogen Chloride (HCl)	4625.2	Roth
Isopropanol 100%	20842.33	VWR
Isopropanol 100%	33539	Honeywell
L-Ascorbate-2-Phosphate	A8960-5G	Sigma
Magnesium Chloride	KK36.2	Carl Roth
Methanol >99% (MetOH)	20847.307	VWR
N-Acetyl-L-Cyteine	4126.2	Carl Roth
Papain from papaya latex	P4762	Sigma
Paraformadehyde	335.2	Carl Roth
Penicillin/Streptomycin (P/S)	P0781	Sigma
Resazurin Sodium Salt	199303-1G	Sigma
Roti Aqua Phenol	A980.3	Carl Roth
Safranin-O	T129.1	Carl Roth
Sodium Acetate	X891.2	Carl Roth
Sodium Chloride	S7653-1KG	Sigma
Sodium Chloride	S7653	Sigma
Sodium Ethylene Diamine Tetraacetatic Acid (Na-EDTA)	8043.2	Roth
Sodium Hydroxide (NaOH)	T135.1	Carl Roth
Sulforhodamine B Sodium Salt	S1402-1G	Sigma
Trisamine (Tris) Base, >99%, p.a.	T1503-1KG	Sigma
Trisaminomethan	AE15.1	Roth
Trizol QIAzol Lysis Reagent	79306	Qiagen
Trypan Blue	CN76.1	Roth

Trypsin/EDTA	T3924	Sigma
Glycine, >99%, p.a.	A1067.5000	AppliChem
Guanidine Hydrochloride	G3272	Sigma
Guanidine Thiocyanate	0017.1	Carl Roth
Hoechst 33342	14533-100MG	Sigma
Hyaluronic Acid Sodium	53747	Sigma
Hydrogen Chloride (HCl)	4625.2	Roth
Isopropanol 100%	20842.33	VWR
Isopropanol 100%	33539	Honeywell
L-Ascorbate-2-Phosphate	A8960-5G	Sigma
Magnesium Chloride	KK36.2	Carl Roth
Methanol >99% (MetOH)	20847.307	VWR
N-Acetyl-L-Cyteine	4126.2	Carl Roth
Papain from papaya latex	P4762	Sigma
Paraformadehyde	335.2	Carl Roth
Penicillin/Streptomycin (P/S)	P0781	Sigma
Resazurin Sodium Salt	199303-1G	Sigma
Roti Aqua Phenol	A980.3	Carl Roth
Safranin-O	T129.1	Carl Roth
Sodium Acetate	X891.2	Carl Roth
Sodium Chloride	S7653-1KG	Sigma
Sodium Chloride	S7653	Sigma
Sodium Ethylene Diamine Tetraacetatic Acid (Na-EDTA)	8043.2	Roth
Sodium Hydroxide (NaOH)	T135.1	Carl Roth
Sulforhodamine B Sodium Salt	S1402-1G	Sigma
Trisamine (Tris) Base, >99%, p.a.	T1503-1KG	Sigma
Trisaminomethan	AE15.1	Roth
Trizol QIAzol Lysis Reagent	79306	Qiagen
Trypan Blue	CN76.1	Roth
Trypsin/EDTA	T3924	Sigma

2.1.2. Buffers, medium, and solutions

A comprehensive list of buffers, medium, and solutions used in this study is provided in Table 2.2.

Buffers/Mediums/Solutions	Compounds and handling
Calcein AM stock solution	502 µl DMSO 1 mg Calcein AM
Trypan blue solution	62.5 mg Trypan blue 50 ml Dulbecco's PBS
Alcian blue solution (1%, PH 2.5)	500 mg Alcian blue (8 GX) 50 ml Acetic Acid (3%)
Guanidine Hydrochloride (6 M)	28.65 mg Guanidine Hydrochloride 50 ml ddH_2O
Safranin-O solution (0.1%)	50 mg Safranin-O 50 ml ddH_2O
Formaldehyde (4%)	Formaldehyde (37%) in ddH_2O
AP Activity Assay buffer (PH 10.5)	3.75 g Glycine 12.11 g Tris-Base 95.21 mg $MgCl_2$ 1 L ddH_2O
PCR loading buffer	25 mg Bromphenol blue 5 ml 10X TBE 5 ml Glycerol (20%)
10 X TBE buffer	108 g TRIS 55 g Boric acid 40 ml EDTA (0.5 M, PH 8) 1 L ddH_2O
Ethanol solution (70%)	99% Ethanol in ddH_2O
Sodium Acetate solution (3M, PH 5)	12.3 g Sodium Acetate in 50 ml

Table 2.2: Buffers, medium, and solutions.

	ddH_2O
Acetic Acid Solution (1%)	100% acetic acid in ddH_2O
Acetic Acid Solution (3%)	100% acetic acid in ddH_2O
TRIS Solution (10 mM)	1.2g TRIS in 1L ddH_2O
SRB Solution	0.4% SRB in 1% acetic acid
Steinberg's Solution	60 mM NaCl 0.7 mM KCl 0.8 mM MgSO4 · 7H2O 0.3 mM CaNO3 · 4H2O 1.4 mM Tris base pH 7.4
Resazurin stock solution	0.025% in DPBS
Resazurin working solution	10% Resazurin stock solution in DPBS
PBE Buffer (PH 6.5)	6.5 mg N-Acetyl-L-Cysteine 138 mg Disodium hydrogen phosphate 14.9 mg EDTA Adjust PH to 6.5 with NaOH Adjust volume to 20 ml with ddH_2O
Papain stock solution (5 mg/ml)	5 mg papain from papaya latex 1 ml PBE buffer
Papain working solution (25 µg/ml)	5 mg/ml stock solution in PBE buffer
DMMB solution buffer (PH 3)	304 mg Glycine 160 mg sodium chloride 9.5 ml 0.1 M Acetic acid 90.5 ml ddH_2O
DMMB stock solution (8 mg/ml)	8 mg DMMB in 1 ml buffer
DMMB working solution (16 µg/ml)	8 mg/ml stock solution in DMMB buffer
Chondroitin Sulfate Standards stock solution	10 mg Chondroitin Sulfate Standards in 10 ml PBE buffer

(1 mg/ml)	
Chondroitin Sulfate Standards working solution (100 µg/ml)	1 mg/ml stock solution in PBE buffer
TE buffer (PH 7.5-8.0)	10 mM Tris base 1 mM EDTA
Calf Thymus DNA stock solution (1 mg/ml)	1 mg Calf Thymus DNA in 1 ml TE buffer
TNE buffer (PH 7.4)	121.1 mg Tris Base 37.2 mg EDTA 1.17 g sodium chloride Adjust PH to 7.4 with HCl Adjust volume to 100 ml with ddH_2O
Chondrocyte Cells Culture Medium	500 ml DMEM +500 ml Ham's F12 +50 ml FCS +10 ml Penicillin/Streptomycin +50 µl L-Ascorbic-2-Phosphate

2.1.3. Consumables

A comprehensive list of consumables used in this study is provided in Table 2.3.

Table 2.3: List of consumables

Consumable	Manufacturer	Type	Serial number
Cover glass	Thermo Fisher Scientific	15 mm	00471782
Cell culture plate	Greiner bio-one	96-well, flat bottom	655180
Cell culture plate	Greiner bio-one	96-well, V bottom	651101
Cell culture plate	Corning.	48-well, flat bottom	3548
Cell culture plate	Greiner bio-one	24-well, flat bottom	662160
Cell culture plate	Corning	6-well, flat bottom	353046
Cell Star Tubes	Greiner bio-one	50 ml	227261
Cell Star Tubes	Greiner bio-one	15 ml	188271
Eppendorf tube	Sarstedt	0.5 ml, white	72.699
Eppendorf tube	Carl Roth	1.5 ml, white	4182.1
Eppendorf tube	Carl Roth	1.5 ml, blue	4190.1
Eppendorf tube	Carl Roth	1.5 ml, green	4209.1
Eppendorf tube	Carl Roth	1.5 ml, red	4189.1
Eppendorf tube	Carl Roth	1.5 ml, yellow	4204.1
Eppendorf tube	Eppendorf	2.0 ml, white	2549
Infusion tubing	Braun	180cm	00412895
Pipette Tips	Sorenson BioScience	0.1 - 10 µl	Colorless
Pipette Tips	Sarstedt	2 - 200 µl	Yellow
Pipette Tips	Ratiolab	100 - 1000 µl	Blue
Silicon strip	Tesa Silikonband	Xdtreme Conditions	4600

Single-channel Pipette	Corning	10-100 µl	158240031
Single-channel Pipette	Corning	20-200 µl	158250088
Single-channel Pipette	Corning	100-1000 µl	058261237
Single-channel Pipette	Eppendorf	0.1-2.5 µl	P35434B
Spectrophotometer	BMG Labtech	Fluostar Omega	415-1264
Water-bath	Lauder Dr. R. Wobser	Al 25	LCB 0727-11-0094
Water-bath	Lauder Dr. R. Wobser	ECO ET 20	LY 06.1

2.1.4. Equipment

A comprehensive list of equipment used in this study is provided in Table 2.4.

Table 2.4: List of equipment.

Equipment	Manufacturer	Type	Serial number
Agitator,magnetic stirrer	IKA-Werke	RH B2	06.050357
Agitator,magnetic stirrer	Heidolph Instruments	MR Hei-Mix L	040700340
Centrifuge	Dako Deutschland	Stat Spin	620E50000693
Centrifuge	Thermo Fisher Scientific	Megafuge 40 R	41307652
Centrifuge	Scientific Industries	SI DD 58	DD58-1001
Centrifuge (Mirco)	Labnet International	BN 08060235	C1301B
Centrifuge (Mirco)	HERAEUS Med	Fresco 17	41250019
Electrophoresis power supplies	Bio-Rad Laboratories	Power Pac 200	285BR05538
Freezer -20℃	BSH	IQ500	GS51NYW41 (01)
ES generator	Vanquish Innovation	#7	6D07
Freezer -20℃	Liebherr	Med Line	LGex3410-21K 001
Freezer -80 ℃	Thermo Fisher Scientific	905	827860-2521
Freezer -86 ℃	Revco	ULT1386-9-V17	R10G-333095-RG
Fridge +4 ℃	Liebherr	Comfort	3523-21L
Fridge +4 ℃	Cool Compact Kühlgeräte G	HKMT 040-01	CC00412514
Ice maker	Scotsmen	AF 80	DD 8837 11 X
Incubator	Thermo Fisher Scientific	Heratherm OMS 60	41296334

Incubator	Binder	9040-0078	11-22649
Incubator	Binder	9040-0081	11-22190
Laboratory pump (Bench)	Carl Roth	Cyclo 2	1109-065
Microscope	PeqlabBiotechnologie	EVOS-fl	91-AF-4301
Mixer	Corning	Vortex Mixer	804995
Mixer	Labinco	LD-76	76000
Multichannel Pipette	Corning	5-50 µl	151620022
Multichannel Pipette	Corning	20-200 µl	551630277
Multichannel Pipette	Thermo Electron	0.5-10 µl	CH98998 4510
Multichannel Pipette	Corning	50-300 µl	151640033
PCR thermal cyclers	Thermo Fisher Scientific	Arktik	10040953
PCR thermal cyclers	Applied Biosystems	Forschungslabor	50132
pH meter	Mettler-Toledo	Five Easy FE 20	1232315296
Pipette controller	Integra	Pipetboyacu	629619
Pipette controller	Heathrow Scientific	Rota-Filler 3000	HSA05119
Refrigerator	Cool Compact Kühlgeräte G	HKMT 040-01	CC 00412516
Refrigerator	Cool Compact Kühlgeräte G	HKMN 062-01	CC 00412513
Safety workbench	Thermo Fisher Scientific	Maxisave S20201.8	41293949
Safety workbench	Thermo Fisher Scientific	Maxisave S20201.8	41293948
Scale	Kern & Sohn	ABJ 120-4M	WB 1140084
Shaker, laboratory	LTF Labortechnik	DRS 12	11DE243
Shaker, laboratory	PeqlabBiotechnologie	ES-20	010111-1107-0119
Shaker, laboratory	LTF Labortechnik	DRS 12	11DE090
Shaker, Laboratory	Corning	LSE Vortex Mixer	1101260

Single-channel Pipette	Corning	0.5-10 µl	158220060
Single-channel Pipette	Corning	2-20 µl	158230441
Single-channel Pipette	Corning	10-100 µl	158240031
Single-channel Pipette	Corning	20-200 µl	158250088
Single-channel Pipette	Corning	100-1000 µl	058261237
Single-channel Pipette	Eppendorf	0.1-2.5 µl	P35434B
Spectrophotometer	BMG Labtech	Fluostar Omega	415-1264
Temperature sensor	HOBO	Data Loggers	1-800-LOGGERS
Water-bath	Lauder Dr. R. Wobser	Al 25	LCB 0727-11-0094
Water-bath	Lauder Dr. R. Wobser	ECO ET 20	LY 06.1

2.2. Methods

2.2.1. The ES system and EF application

In general, the novel experimental system required distributing the EF signals generated by an EF generator (Vanquish Innovation, New York, U.S.A.) uniformly to four ES areas (Figure 2.1.C.). Moreover, it shall avoid inherent defects of direct coupling stimulation mentioned before.

The experimental system for cell culture and ES (Figure 2.1.) was adapted to standard 6-well culture plates (Corning Costar, Merck, Darmstadt, Germany) (Lu *et al.*, 2021), and the principle was based on previous research (Song *et al.*, 2007). The system consisted of two main parts: a 6-well culture plate, which holds four ES chambers (Figure 2.1.A), and a custom-made lid (Figure 2.1.B).

Anodes and cathodes were served by the two middle wells (well No. A2 and well No. B2) of the 6-well plate (Figure 2.1. A), whereas the other four wells were modified as the ES areas (wells No. A1, A3, B1, and B3) (Figure 2.1.C). To initiate the stimulation, wells No. A2 and B2 were filled with 8 mL Steinberg's solution (salt-conducting), and 4 mL HaCaT cell culture medium (Dulbecco's Modified Eagle Medium, DMEM, Life Technologies, Darmstadt, Germany) was added to the remaining four wells (ES areas) (Lu *et al.*, 2021).

The ES areas (Figure 2.1.D) were divided into two reservoirs with reservoir walls (made of plastic strips, tinted green in Figures 2.1.A and D) and an electrotactic chamber (hereafter ‘chamber’) (Figure 2.1.C). The chamber is the core component of the ES system. It consists of two parts: the chamber wall and the ceiling. A plastic ring made from a cap of 15 mL Falcon tube (length, 2.0 cm; height, 1.0 cm; blue part in Figures 2.1.A, C, and D) served as the chamber wall, where two windows (2.0 mm high × 5.0 mm wide) were carved on opposite sides to ensure permeability of the medium, as well as the EF signal (Lu *et al.*, 2021).

To maintain an even potential difference and reduce the Joule heating effect, it was essential to keep the height of the chamber low (Song *et al.*, 2007). Therefore, a chamber ceiling was required. The ceiling was a smaller threaded plastic ring (salvaged from the main body of a 15 mL Falcon cylinder) with a round cover glass (diameter, 15 mm; Thermo, Braunschweig, Germany) fixed at the bottom

(Figure 2.1.D). As the wall and the ceiling were obtained from a Falcon cylinder, the ceiling could easily be screwed into the chamber wall. Therefore, the cover glass of the ceiling could maintain the height of the chamber at 0.5 mm (Figure 2.1.C) (Lu *et al.*, 2021).

The custom-made lid (Figure 2.1.B) was adapted to the lid of a standard 6-well plate. Eighteen holes (diameter, 0.5 cm) were pre-drilled in the lid to fix two silver rods and eight agar bridges. This was a crucial parallel structure to ensure the potential difference was distributed evenly via agar bridges, which connected the anode (well No. A2) and cathode (well No. B2) with the reservoirs of each ES area.

The agar bridges were manufactured using a segment of infusion tubing (length, 15.0 cm; diameter, 0.5 cm; Braun, Melsungen, Germany) filled with sterile 2% agarose LE (J.T. Baker, Mansfield, MA) diluted in Steinberg's solution. Application of the agar bridges can transmit the EF signals and isolate harmful substances (Hamburger, 1942).

Two silver electrodes (length, 5.0 cm; diameter, 0.5 cm) were connected to the EF generators and inserted into the anode (well No. A2) and cathode (well No. B2) via the middle two holes of the lid (Figure 2.1.A).

Before each experiment, cells were cultured on round collagen-coated coverslips (diameter, 15 mm; Thermo, Braunschweig, Germany) and placed in the middle of the ES areas. Then, the ceilings were screwed into the chamber wall (Figure 2.1.C). Afterward, the lid (Figure 2.1.B) was mounted to close off the experimental system (Figure 2.1.A). The following two conditions were required to maintain EFs of 200 mV/mm within each chamber: **a**. agar bridges were spaced 35 mm apart from each other, and **b**. the EF generator provided a continuous potential difference of 7 V (Lu *et al.*, 2021).

In this way, each of two agar bridges in an ES area would be connected to one reservoir, one anode (No. A2) or another reservoir and cathode (No. B2), and the identical EF signals could be distributed to the four chambers in parallel. In other words, an identical potential difference was delivered through the agar bridges to the respective reservoirs in each ES area, therefore building EFs on HaCaT cells (Lu *et al.*, 2021).

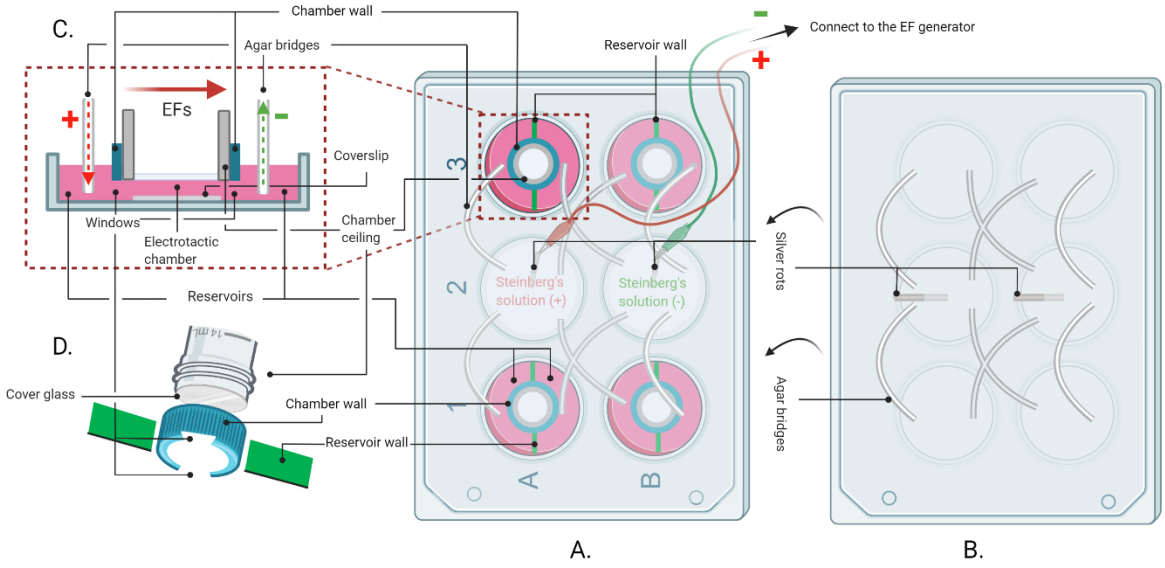

Figure 2.1. Diagrammatic description of the experimental ES system. (A) Top view of the assembled experimental ES system. (B) Scheme of the custom-made lid. (C) Side view of the ES areas. (D) Components of the electrotactic chamber. (Lu *et al.*, 2021) *Created with BioRender.com*

The stability of temperature and pH are essential factors affecting cell culture (Song *et al.*, 2007). Therefore, we assessed the change of these two parameters in the ES system within 72 hours in the presence of the EFs (200 mV/mm). The pH was measured by a pH meter (Mettler-Toledo, Greifensee, Switzerland), and the temperature was measured by a temperature sensor (HOBO, South Burlington, USA).

2.2.2. Scratch wound closure assay

In the conventional approach for the scratch wound closure assay (hereafter 'scratch assay'), linear scratches were made with sterile pipette tips (Liang *et al.*, 2007). This would inevitably cause cell fragments to be generated and piled on the edge of the scratch, interfering with accurate gap measurement (Figure 2.2.A). Thus, we used a novel method to perform the scratch assay in this study (Lu *et al.*, 2021).

In brief, sterile self-adhesive silicone strips (length, 10.0 mm; width, 0.3 mm. Tesa Silikonband, Offenburg, Germany) were used to generate the cell-free areas

(equal to the scratches). The strips were adhered to the round collagen-coated coverslips (diameter, 15 mm; Thermo, Braunschweig, Germany) to prevent the entrance of cells (Lu *et al.*, 2021).

HaCaT cells were then seeded on the coverslips in a 24-well plate (Corning Costar, Merck, Darmstadt, Germany) at a density of 5.0×10^4 cells/cm^2 in DMEM. After attachment of the cells (approximately 3-5 hours), silicone strips were carefully removed with fine sterilized tweezers, and neat cell-free areas were generated (Figure 2.2.B). Afterward, the coverslips were transferred to the electrotactic chambers of the ES areas. The system was assembled as described previously, and ES was initiated (Lu *et al.*, 2021).

The system was transferred to a cell culture incubator (5% CO_2 at 37°C, Heraeus 6000 Thermo Fischer Scientific, Langenselbold, Germany). To monitor cell migration, a microscope (Carl Zeiss, Oberkochen, Germany) with 20× magnification was used, and three images per ES area were taken in 12 hours intervals for the 36-hour incubation period (Lu *et al.*, 2021).

Images were evaluated with ImageJ software (NIH, Bethesda, MD, USA), and the migration rate was calculated according to the following formula (Ehnert *et al.*, 2018a):

$$\text{Migration Rate} = \frac{\text{Cell Free Area}(0\ \text{Hour}) - \text{Cell Free Area}(\text{n Hour})}{\text{Cell Free Area}(0\ \text{Hour})} \times 100\%\ , \text{n} = 0,12,24, \text{and } 36$$

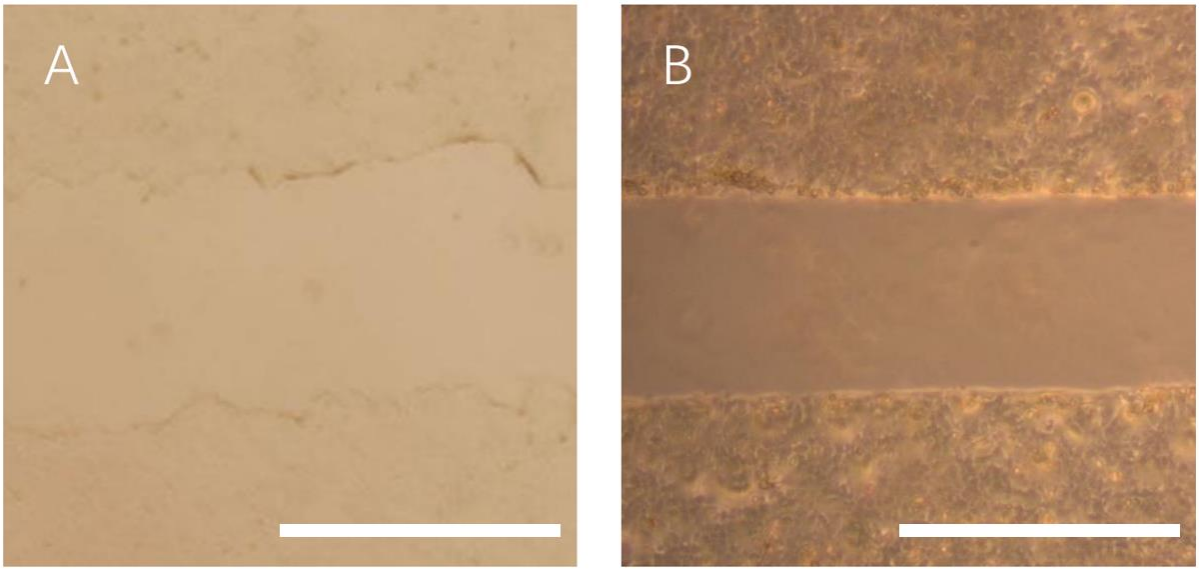

Figure 2.2. Comparison of the conventional scratch assay and the newly developed method. A. Image using the conventional approach, B. Image using the newly developed method. *Scale bar: 400 µm*

2.2.3. Resazurin conversion assay

Cell proliferation for ES treatment of HaCaT cells was evaluated via a resazurin conversion assay. Briefly, at days 1, 4, and 7 after exposure, the supernatant of HaCaT cells was discarded, and the cells were washed twice with Dulbecco's Phosphate Buffered Saline (DPBS), 0.0025% resazurin solution (w/v, in DPBS, Sigma-Aldrich, Darmstadt, Germany) was added to the cell culture at 5% CO_2, 37°C for 60 min (Lu *et al.*, 2021). The fluorescence intensity of resorufin in the liquid was measured with a plate reader (Omega, BMG Labtech, Ortenberg, Germany) at ex/em = 540/590 nm, and the background readouts were deducted from the results as previously described (Ehnert *et al.*, 2018b).

2.2.4. Sulforhodamine B (SRB) staining

The sulforhodamine B (SRB) assay was used to determine cellular total protein content, again reflecting cell proliferation (Skehan *et al.*, 1990). To use the SRB assay to determine the effect of ES treatment on HaCaT cells, the supernatant of HaCaT cells was discarded on days 1, 4, and 7 after exposure (Lu *et al.*, 2021). After washing twice with DPBS, ethanol fixation (–20°C, overnight) was used to

ensure homogenous permeability of HaCaT cells to the dye. Afterward, fixed cells were stained in SRB solution (0.4% w/v SRB in 1% acetic acid, Sigma-Aldrich, Darmstadt, Germany) at RT for 30 min. Next, the HaCaT cells were rinsed with 1% acetic acid 4–5 times to remove the unbound SRB and air-dried. Bound SRB was solubilized with 10 mM unbuffered Tris solution (pH 10.5, Sigma-Aldrich, Darmstadt, Germany) (Lu *et al.*, 2021). Subsequently, the resolved SRB absorbance was qualified at 565–690 nm wavelength.

2.2.5. Quantification of total DNA content

DNA extraction and quantification were achieved as previously described (Meeker *et al.*, 2007). Briefly, HaCaT cells that underwent different EF exposure times (days 1, 4, and 7) were washed twice with DPBS, lysed in 50 mM NaOH at 98°C for 5 min, and the samples were stored at −20°C for at least 12 hours for maximum yield of DNA. After thawing the samples at room temperature, 200 µL of 100 mM Tris buffer (pH 8.0) was added to each sample to neutralize the pH. To remove insoluble cell fragments, the samples were centrifuged at 14 000 × g for 10 min at 4°C (Lu *et al.*, 2021). Supernatants were then transferred into fresh Eppendorf tubes. Total DNA content was quantified photometrically at 260 nm via the plate reader (Ehnert *et al.*, 2019b).

2.2.6. Calcein AM staining and Hoechst staining

Living cells were visualized by calcein AM (green fluorescence, Sigma-Aldrich, Darmstadt, Germany). Nuclei were labeled by Hoechst 33,342 (blue fluorescence, Sigma-Aldrich, Darmstadt, Germany) (Lu *et al.*, 2021). Briefly, after reaching the ES exposure time points (1 and 7 days), HaCaT cells were washed three times with DPBS and incubated with calcein AM (2 µM) and Hoechst 33,342 (1 mg/mL). The samples were shaken on a shaker for approximately 30 min, protected from light (Lu *et al.*, 2021). After that, images were captured via an epifluorescence microscope (EVOS FL, Life Technologies, Darmstadt, Germany) (Aspera-Werz *et al.*, 2020).

2.2.7. Growth factor expression measurement

We used the RayBio Human Growth Factor Array (RayBiotech, Norcross, GA,

USA) to investigate the expression of healing-related growth factors at the protein level (Lu *et al.*, 2021). Experiments were performed strictly following the manufacturer's protocol.

Briefly, growth factor array membranes were washed with the washing buffer (provided in the kit) and incubated in blocking buffer (provided in the kit) at RT for 2 hours. Meanwhile, the culture supernatant samples of the ES group (exposure time 7 days) and the control group were collected. Next, the membranes were incubated with the supernatant of different groups respectively at 4°C overnight. After incubation, the membranes were rinsed with washing buffer and incubated with a primary biotin-labeled antibody (provided in the kit, RT, 1.5 hours) and HRP-streptavidin (provided in the kit, RT, 1.5 hours) successively (Lu *et al.*, 2021). To develop the HRP signals, the membranes were subsequently washed with enhanced chemiluminescence (ECL) solution (provided in the kit). Chemiluminescence was detected using an ECL ChemoCam Camera (INTAS Science Imaging Instruments, Goettingen, Germany). Relative expressions, normalized to the POS (positive control) and NEG (negative control) dots on the membranes, were quantified densitometrically via ImageJ software (Version 1.8.0_172, NIH, Bethesda, MD, USA) (Ehnert *et al.*, 2019a).

2.2.8. Western blot

Western blot analysis was performed as previously described (Ehnert *et al.*, 2015). In brief, HaCaT cells in each group were washed with ice-cold DPBS and then lysed according to the lysis protocol in the ice-cold radioimmunoprecipitation assay. Protein concentration was determined using the Micro-Lowry assay (Lowry *et al.*, 1951).

Next, 25 µg total protein was loaded onto sodium dodecyl sulfate−12.5% polyacrylamide gel for electrophoresis and transferred onto nitrocellulose membranes. Nonspecific binding sites on the membranes were blocked with 5% bovine serum albumin (BSA) solution for 60 min at RT; subsequently, the membranes were incubated with respective primary antibodies (Cell Signaling, Beverly, USA) diluted in Tris-buffered saline/Tween 20 (TBS-T; 1:1000) at 4°C overnight (Lu *et al.*, 2021). The following day, the membranes were incubated

with the HRP-conjugated secondary antibody (Cell Signaling, Beverly, USA, 1:10 000 dilutions in TBS-T) for 2 hours at RT. Following triple washes in TBS-T, the membranes were incubated with ECL for 1 min (Lu *et al.*, 2021).
Immunoblots were developed using the ECL ChemoCam. Densitometric analysis of band intensities was evaluated using ImageJ software (Lu *et al.*, 2021). Expression levels of the proteins were normalized to glyceraldehyde 3-phosphate dehydrogenase (GAPDH) expression levels (Wang *et al.*, 2014).

2.2.9. Statistics

GraphPad Prism software 9.0.0 (El Camino Real, CA, USA) was used to analyze the results; data are displayed as mean ± SEM ($N \geq 3$, $n \geq 3$). The differences between multiple groups were estimated by a nonparametric two-way ANOVA followed by Tukey's multiple comparison test, or a Kruskal-Wallis test. The two groups' differences were estimated by a Mann-Whitney U test (Lu *et al.*, 2021).
The hypotheses of the two-way ANOVA were as follows: H0: The means of the ES groups and non-ES groups are equal; H1: The means of the ES groups and non-ES groups are different. (Result 3.2, Result 3.3, Result 3.7)
The hypotheses of the Mann-Whitney U test were as follows: H0: The secretion function of the ES groups and non-ES groups are equal; H1: The secretion function of the ES groups and non-ES groups are different. (Result 3.4)
The hypotheses of the Kruskal-Wallis test were as follows: H0: the mean ranks of the different timepoints groups are the same; H1: the mean ranks of the different timepoints groups are different. (Result 3.5, Result 3.6)
Statistical significance was determined as $p \leq 0.05$. Data and statistic methods are verified and published in Life-Basel (Lu *et al.*, 2021).

3. Results

3.1. Reliability of the experimental ES system

Compared to the work of pioneers, our newly designed experimental ES system simplified the structure and improved the reliability (Song *et al.*, 2007, McCaig *et al.*, 1994, Pelletier *et al.*, 2015, Rajnicek *et al.*, 2018, Koppes *et al.*, 2011). Moreover, it allowed up to four ES areas to receive identical EF signals simultaneously (Figure 3.1.A), which dramatically increased the repeatability and reliability of the system.

pH value and temperature are critical to the cell culture environment. A total of 72 hours of continuous monitoring was performed, and the result showed that, in the continuous presence of EFs (200 mV/mm), pH value (Figure 3.1.B) and temperature (Figure 3.1.C) could be maintained at a viable level for cell culture, and this suggested that a stable culture environment could be kept up between two medium changes (Lu *et al.*, 2021).

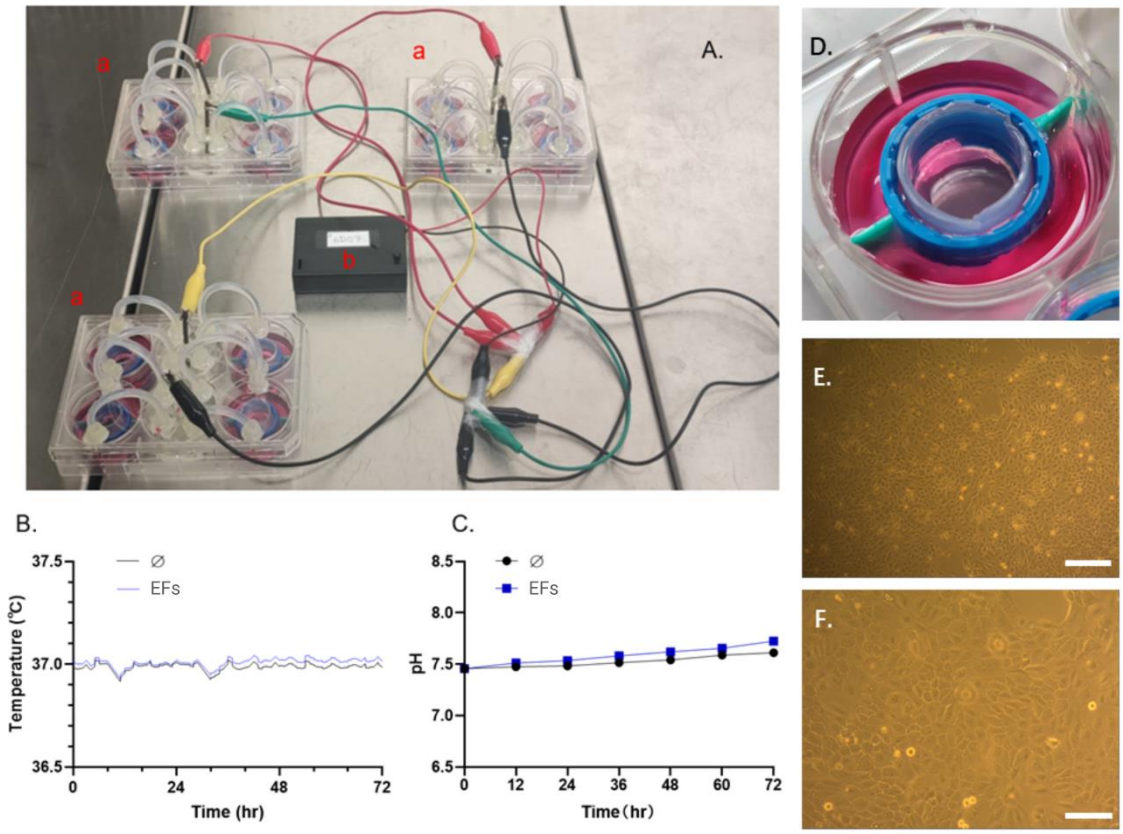

Figure 3.1 Temperature and pH value could be maintained at a stable level for 72 hours in the presence of EFs. (A) Photograph of three ES systems during work at the same time: a. Four ES areas of each system received identical EF signals simultaneously, b. EF generator. (B) Compared with the control group, the ES group's temperature change did not exceed 0.1°C. (C) Compared with the control group, the ES group's pH change did not exceed 0.2. (D) Image of the ES area. (E) and (F) demonstrated that the ES area affords an excellent light transmission for observation. Representative images showed (E) HaCaT cells were cultured in the ES area. Magnification 40×, scale bar 200 μm. (F) HaCaT cells were cultured in the ES area. Magnification 100×, scale bar 80 μm (Lu *et al.*, 2021).

3.2. ES promotes HaCaT cell migration

To address the role of EFs in wound healing *in vitro*, the scratch assay was performed to evaluate the influence of the absence or presence of EFs on HaCaT cell migration (Lu *et al.*, 2021). The cells were stimulated and imaged in the absence or presence of EFs in 12 hours intervals for a 36-hour incubation period. The scratch assay demonstrated that ES significantly increased the wound closure rate beginning 24 hours after exposure, showing an improvement up to 46.51% compared to the no-ES groups (Figure 3.2.).

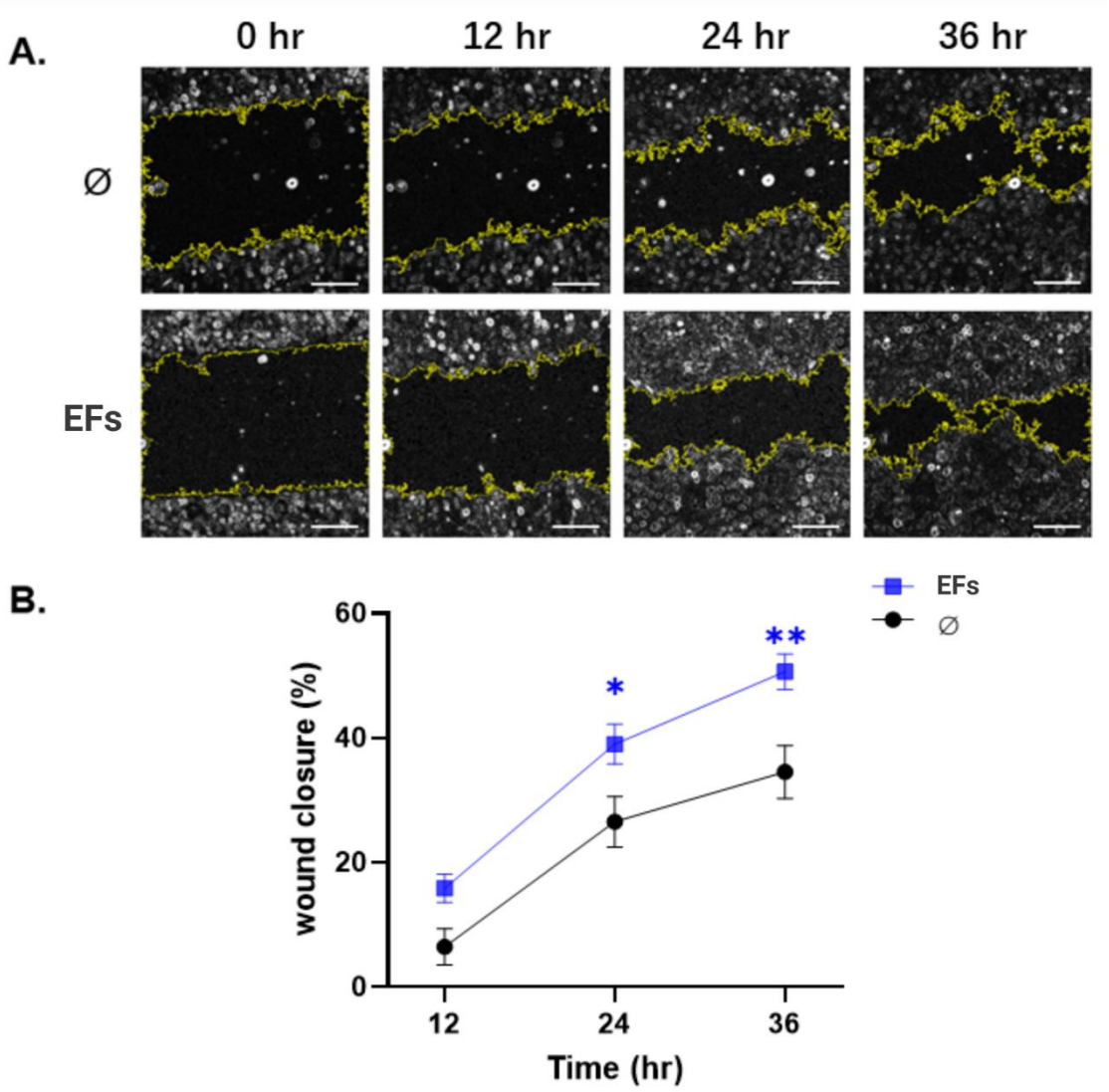

Figure 3.2. The speed of wound closure was accelerated in the ES groups. After 12, 24, and 36 hours of exposure to EFs, the wound closure speed was evaluated. (A) Representative images of the scratch assay. The cell-free areas were measured by ImageJ software. The yellow lines indicate the edges of the cell-free areas. (B) The changes in the scratch area over 36 hours and the cell-free areas at 0 hours were defined as 100%. Scale bar = 100 μm. N = 3, n = 3. Data were analyzed by nonparametric two-way ANOVA, followed by Tukey's multiple comparison: * $p < 0.05$, ** $p < 0.01$ compared with the non-ES groups (Lu *et al.*, 2021).

3.3. Improvement of HaCaT cell proliferation induced by ES application

In order to assess the stimulating effects of EFs on proliferation and cell viability, HaCaT cells were exposed to 200 mV/mm EFs for up to 7 days. Mitochondrial activity (resazurin conversion assay), total protein content (SRB staining), and DNA quantification (total DNA content), which are indirect cell proliferation indicators, were measured, respectively (Lu *et al.*, 2021). At the same time, calcein AM and Hoechst staining were performed to visualize the results (Figure 3.3.).

With EF application, the uptrends of the indicators above were more pronounced during the 7-day experimental period. The mitochondrial activity (up to 26.7%, Figure 3.3.B) and total protein content (up to 21.4%, Figure 3.3.C) on day 7 in the ES groups increased significantly ($p < 0.05$) when compared with those in the non-ES groups. Concerning mitochondrial activity and total protein content, following 7 days of exposure to EFs, a significant increase (up to 17.2%, $p < 0.05$, Figure 3.3.D) of the DNA content could be observed compared with non-ES groups. Calcein AM and Hoechst staining demonstrated a time-dependent increase caused by EFs throughout the experimental period (Figure 3.3.A) (Lu *et al.*, 2021).

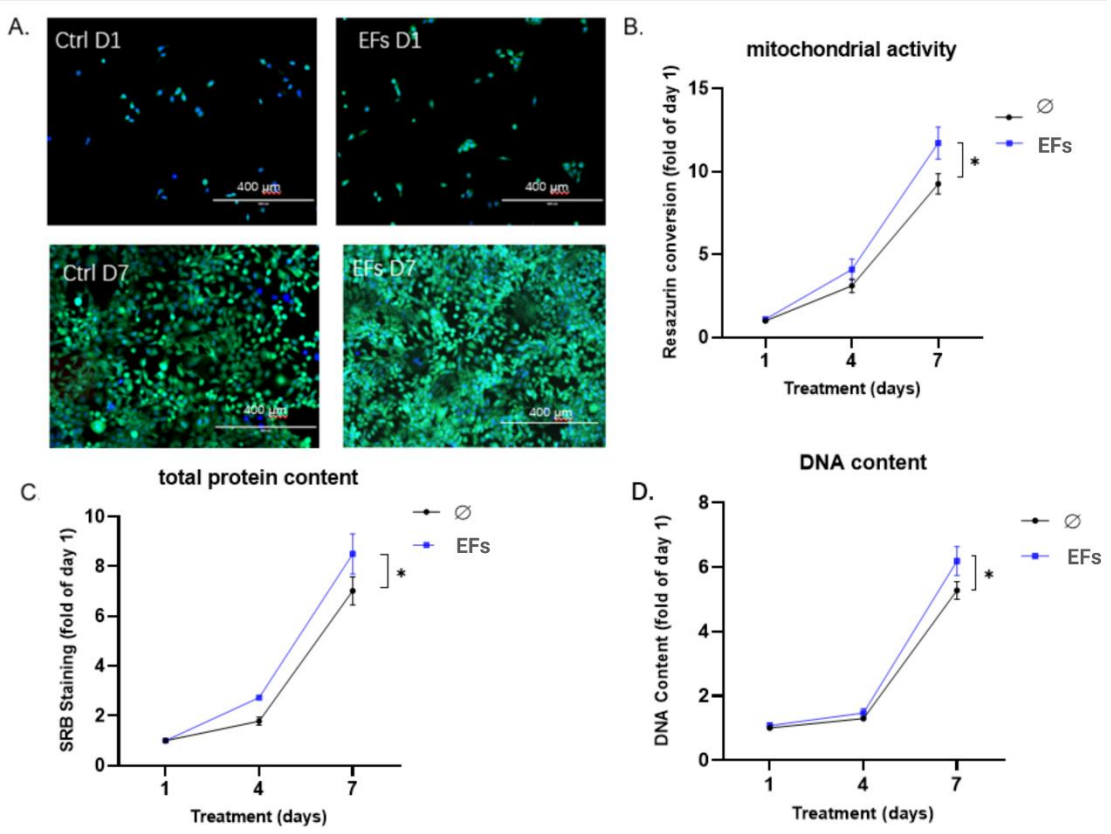

Figure 3.3. Improvement of HaCaT cell proliferation induced by EF application, after 1, 4, and 7 days of EF exposure. (A) Representative images of calcein AM plus Hoechst stainings showed a massive increase of live cells when an electric field was applied. (B) In the same line of evidence, we saw an increase in mitochondrial activity, (C) total protein, and (D) total DNA content after 7 days EF exposure compared to the non-ES groups. Data were analyzed by nonparametric two-way ANOVA, followed by Tukey's multiple comparison test (N ⩾ 3, n = 3; * $p < 0.05$) compared with the non-ES groups (Lu *et al.*, 2021).

3.4. Changes in growth factor expression upon EF exposure

A human growth factor array assay was performed to identify the expression level changes of healing-associated growth factors secreted by HaCaT cells after 7 days of EF exposure (Figure 3.4.A). The results are presented as a heatmap and bar graph (Figure 3.4. B&C) (Lu *et al.*, 2021).

The results demonstrated that several growth factors were increased after EF exposure, with significant increases in granulocyte-macrophage colony-stimulating factor (GM-CSF) and platelet-derived growth factor AB (PDGF-AB)

which are emerging as crucial players in the wound healing process and tissue reconstruction (Barrientos *et al.*, 2008). GM-CSF was the most abundant factor secreted by HaCaT cells (328.07% compared with non-ES groups), followed by fibroblast growth factor-7 (FGF-7; 206.06%) and PDGF-AB (167.31%) compared with non-ES groups (Lu *et al.*, 2021).

Meanwhile, a small number of cytokines (*e.g.,* insulin-like growth factor-binding protein-5) seemed to decrease following ES exposure, although the differences did not reach statistical significance.

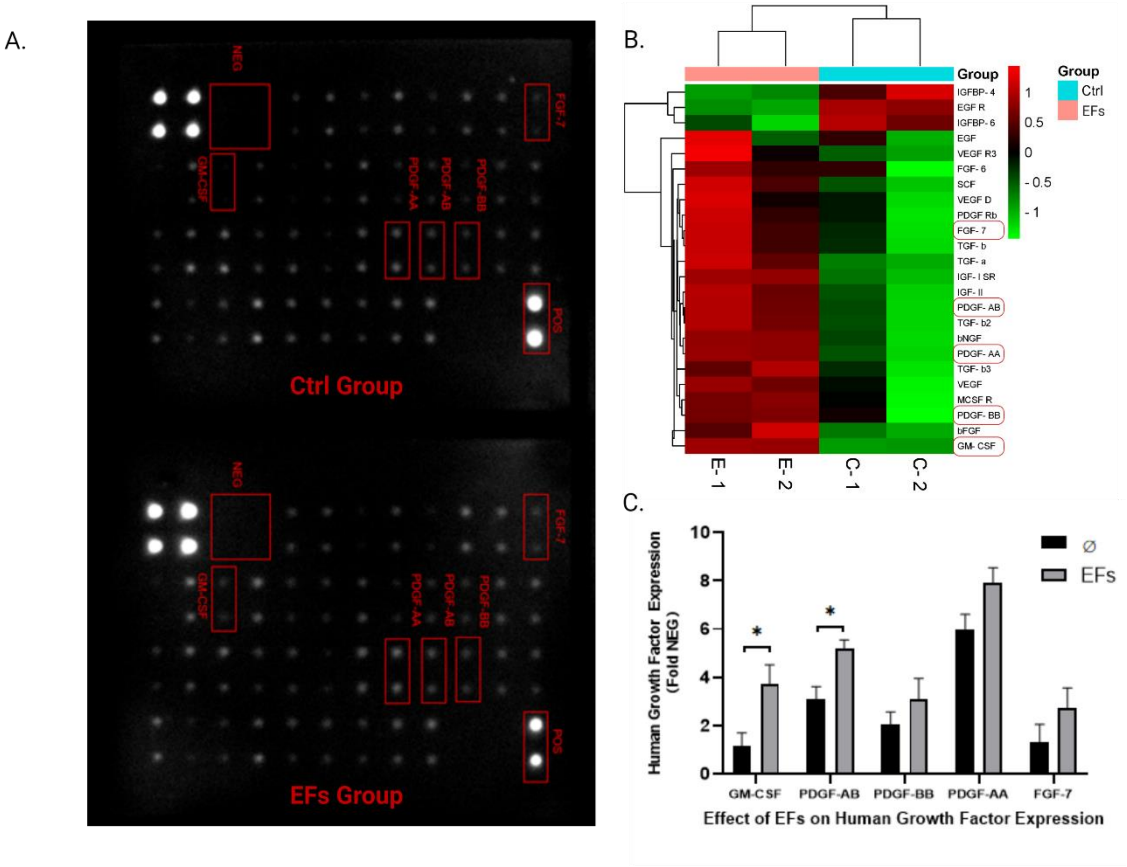

Figure 3.4. Growth factor expression in the ES and non-ES groups after 7 days of EF exposure. (A) Representative images of human growth factor arrays. POS: positive control; NEG: blank control. (B) The expression levels were shown via heatmap (green-black-red), corresponding to lower and higher expression levels. E-1/2 and C-1/2 represent the duplicate measurements of different groups. The five most obviously upregulated factors (compared with the non-ES groups) are shown in red. (C) The signal density was demonstrated as fold of change relative to NEG and compared with that of the non-ES groups. Data were compared using Mann-Whitney U test (N = 3, n = 3; * $p < 0.05$) compared with the control (non-

ES groups) (Lu *et al.*, 2021).

3.5. ERK1/2 is pivotal for responding to ES

3.5.1. ES resulted in enhanced phosphorylation of ERK1/2 and P38 in HaCaT cells.

To investigate the potential molecular mechanism of HaCaT cells responding to ES, phosphorylation levels of several signaling molecules were investigated via Western blot at different timepoints after EF exposure (Figure 3.5.).

The results demonstrated that, following EF exposure, the signals of p-ERK1/2 (approximately +360%, $p \leq 0.0001$) and p-P38 (approximately +260%, $p \leq 0.01$) showed significant increases, with a peak signal at 90 min. We also investigated the phosphorylation levels of phospho-90RSK and phospho-27HSP; however, no pronounced differences were observed.

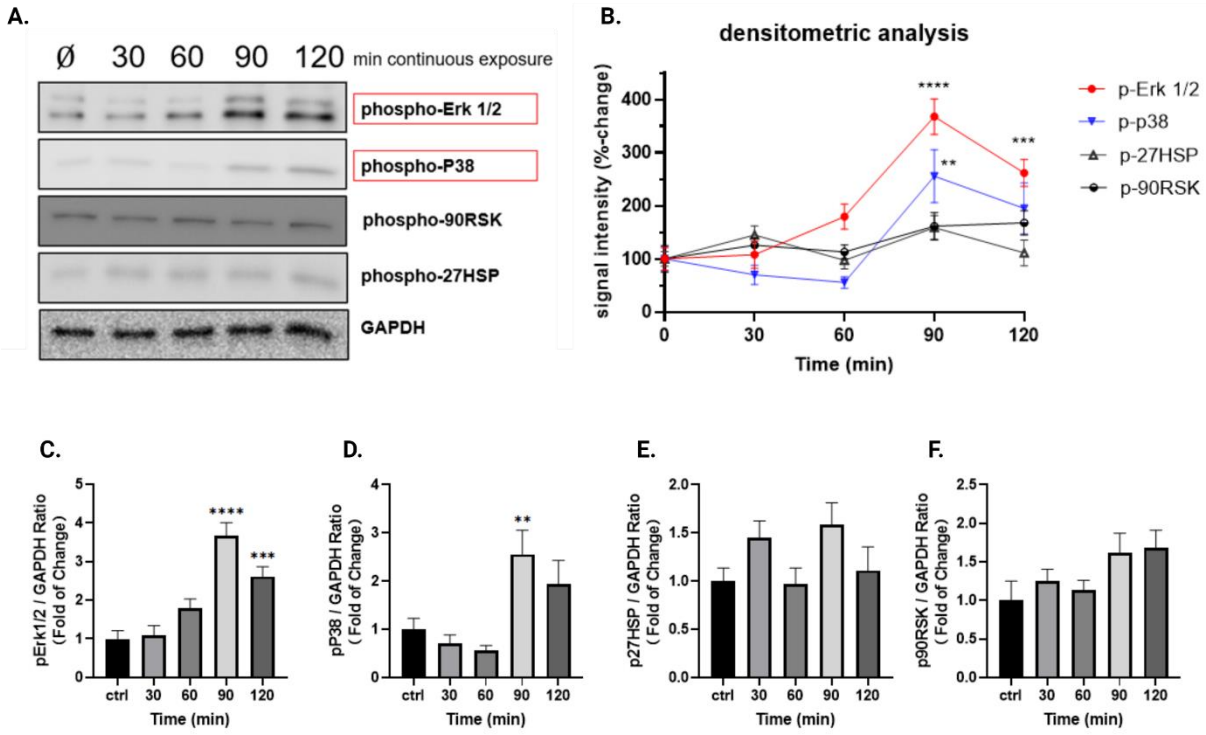

Figure 3.5. Regulation of ERK1/2 and P38 by phosphorylation induced by ES. (A) Representative Western blot images. After 30, 60, 90, and 120 min of EF

exposure, the Western blot signals for p-ERK1/2 and p-P38 increased. The GAPDH expression was used as a loading control. (B) Quantify the protein levels by densitometric analysis of the Western blot by ImageJ software. (C-F) Quantitative analysis of p-ERK1/2, p-P38, p-27HSP, and p-90RSK after EF exposure. Data were compared using Kruskal-Wallis test: N = 3, n = 3; ** $p < 0.01$, *** $p < 0.001$, **** $p < 0.0001$ (Lu *et al.*, 2021).

3.5.2. Toxicity test of signaling pathway inhibitors

To further determine the mechanism of the EF-induced phosphorylation of ERK1/2 and P38 in HaCaT cells migration, the specific signaling pathway inhibitors U0126 (to inhibit ERK1/2) and SB203580 (to inhibit P38) were used. Before this intervention, a toxicity test of inhibitors was performed.

HaCaT cells were treated with different concentrations (1, 2, 5, and 10 μm) of the chemical inhibitors U0126 and SB203580 for 24 hours, and the toxicities were evaluated by resazurin conversion assay and SRB staining. The results demonstrated that mitochondrial activity and total protein content showed no significant difference when inhibitors were used in concentrations that did not exceed 5 μm (Figure 3.6.) (Lu *et al.*, 2021).

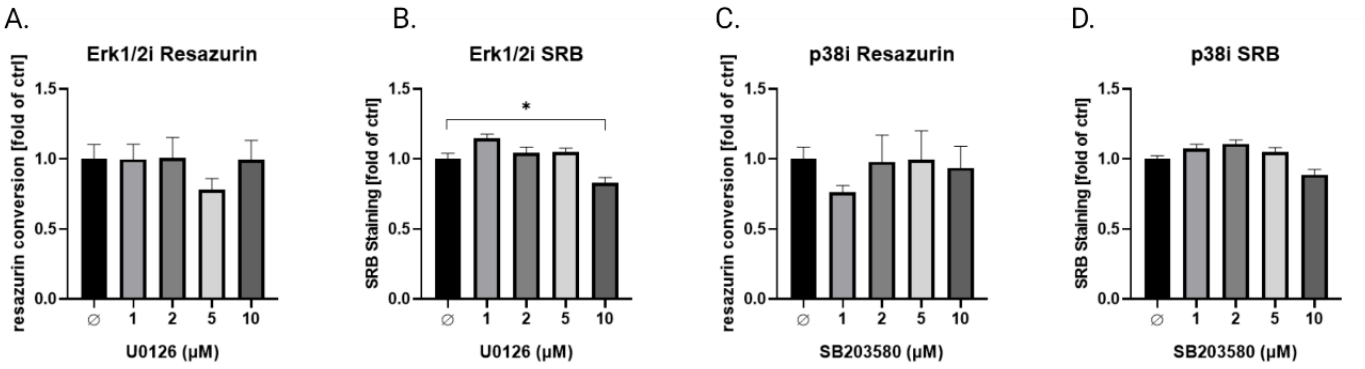

Figure 3.6. Toxicity test of ERK1/2i (U0126) and P38i (SB203580). Mitochondrial activity and total protein content suggested no significant toxicity when inhibitors were used in concentrations not exceeding 5 μm (A. and B.) Influence of different ERK1/2i (U0126) concentrations on the mitochondrial activity and total protein content of HaCaT cells. (C. and D.) Influence of different P38i (SB203580) concentrations on mitochondrial activity and total protein content of HaCaT cells. Data were compared using Kruskal-Wallis's test: N = 3, n = 3; * $p < 0.05$.

3.5.3. ERK1/2 is pivotal for responding to EF-induced migration.

To investigate the EF-induced migration activated by ERK1/2 or P38 signaling, HaCaT cells were cultured in the presence and absence of inhibitors of ERK1/2 (U0126) and P38 (SB203580) signaling, with and without exposure to EFs, and the scratch assay was performed to re-evaluate the cell migration. Results showed that the specific inhibitors of Erk1/2 signaling (U0126) significantly inhibited the cells migration induced by the ES; however, the inhibition of p38 signaling did not influence migration. Collectively, the ES accelerated HaCaT cells' migration by phosphorylating Erk1/2 (Figure 3.7.) (Lu *et al.*, 2021).

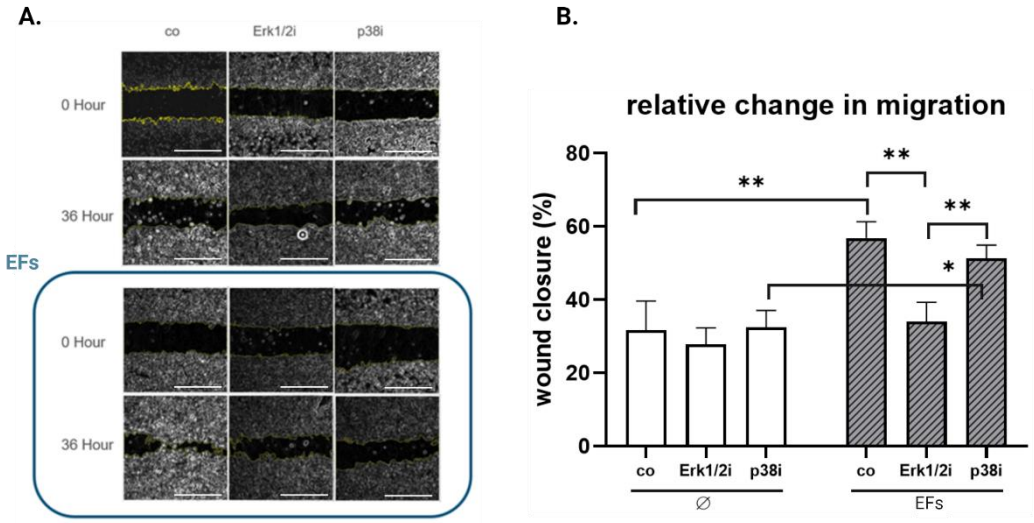

Figure 3.7. To investigate the EFs-induced migration activated by ERK1/2 or P38 signaling, HaCaT cells were cultured in the presence and absence of inhibitors of ERK1/2 (U0126) and P38 (SB203580) signaling, with and without exposure to the EFs. (A.) Representative images of the scratch assay. The edges of the cell-free areas were indicated by yellow lines (scale bar = 400 μm). (B.) Quantification of the scratch assay. Yellow lines indicated the edges of the cell-free areas. Results were analyzed using non-parametric two-way ANOVA followed by Tukey's multiple comparison test: N = 3, n = 3, * $p < 0.05$, ** $p < 0.01$ (Lu *et al.*, 2021).

4. Discussion

Over the past 30 years, increasing evidence has gradually demonstrated that the TEP plays an essential role during the processes of cell division, migration, and differentiation (McCaig *et al.*, 2005, Levin, 2007). More importantly, the therapeutic benefits of the TEP on the nervous system (Shapiro *et al.*, 2005), tumorigenesis (Kirson *et al.*, 2004), and wound healing (Rajnicek *et al.*, 1988) have been confirmed by clinicians. TEP-based devices are also increasingly employed in daily clinical practice (Luo *et al.*, 2021a).

Although the clinical applications of ES in wound healing is promising (Carroll *et al.*, 2000), the mechanisms as to how ES relates to biological effects are still less studied. One of the reasons could be attributed to the lack of a suitable *in vitro* experimental ES system that can effectively deliver the EFs signals to cells (Balint *et al.*, 2013); see Introductuion1.2.3. Hence, in this study, the first issue was establishing an eligible ES system.

4.1. The significance of the novel ES system for *in vitro* study.

To address the difficulty of translating EFs to multi-well plates, we used a standard 6-well cell culture plate as the body part of the ES system, ensuring that identical EFs could be delivered to up to four wells simultaneously (Lu *et al.*, 2021). In contrast to previous studies, which only have one ES area for a single experiment (Rajnicek *et al.*, 2018, Pelletier *et al.*, 2015, Song *et al.*, 2007), this is a significant advancement in improving repeatability. Furthermore, clinical infusion tubes and falcon cylinders were used for easy replication instead of using “tailor-made” glass agar bridges and electrotactic chamber (Song *et al.*, 2007, Cho *et al.*, 2018, McCaig *et al.*, 1994, Lu *et al.*, 2021) to build the ES system, increasing the feasibility of the study. Tests up to 72 hours confirmed that the pH value and temperature in the electrotactic chamber could always be kept suitable between two medium changes, thus meeting the requirements (Song *et al.*, 2007) of a follow-up study.

4.2. Migration and proliferation of HaCaT cells enhanced by ES exposure.

In this study, the HaCaT cell line was selected for investigation. HaCaT cells, as a skin-derived human keratinocyte cell line, are an ideal candidate for the investigation of wound healing (Schoop *et al.*, 1999). This is because their proliferation and migration mimic the critical steps in the skin's wound healing process. In particular, HaCaT cells can sensitively respond to EF stimuli (Cho *et al.*, 2018).

Rapid wound closure occurs in the wound healing process due to the rapid migration of keratinocytes located at the wound margin (Dorschner *et al.*, 2020). Therefore, increased migration of keratinocytes means a potential acceleration of wound healing. In this study, the scratch assay demonstrated that 200 mV/mm EFs significantly accelerated HaCaT cell migration from 12-24 hours, which is following the migration time points of keratinocytes during human wound healing process (Usui *et al.*, 2008, Eming *et al.*, 2009), suggesting that the EFs could be a potential facilitator of wound healing in the early stage. Meanwhile, a study by Ji *et al.* also proved that EFs of 200 mV/mm promote mouse keratinocyte migration via up-regulates MAPK signaling pathway (Ji *et al.*, 2020), which was in line with our research. Moreover, other studies found that physiological EFs in chronic wounds are disturbed and stalled before the re-epithelialization phase of healing (Kloth, 2014), which also provides evidence of the crucial role of EFs in the regulation of cell migration.

Similar to the migration, proliferation of keratinocytes is another cornerstone to close the wound (Handly and Wollman, 2017, Santoro and Gaudino, 2005). In this study, we observed that ES positively affected all proliferation indicators (mitochondrial activity, protein synthesis, DNA synthesis), indicating a crucial role of EFs in accelerating wound healing via improving cell proliferation. These results agree with Cui *et al.,* who observed that EFs (100mV/mm) transimitted via an electrically conductive membrane significantly promoted HaCaT cells proliferation (Cui *et al.*, 2021). Furthermore, another research by Goldman *et al*. demonstrated that EFs significantly improved fibroblast cell proliferation in an *in vitro* chronic wound model (Goldman and Pollack, 1996), suggesting that multiple

cells in the wound site can respond to the EFs signals.

In fact, recent reports have shown that ES accelerates the proliferation of more cell types besides keratinocytes, for instance, cardiomyoblasts (Aragón *et al.*, 2020) and osteoblasts (Vadlamani *et al.*, 2019); however, it is worth noting that excessive cell proliferation can also increase the risk of tumorigenesis. A study by Fedrowitz *et al*. showed evidence that EMFs (electromagnetic fields) facilitate tumorigenesis in a breast cancer model (Fedrowitz and Löscher, 2008). In the same line of evidence, Anderson *et al*. also demonstrated the effect of chronic exposure to 60 Hz EFs on mammary tumorigenesis in the rat (Anderson *et al.*, 1989). Taken together, concerning the application of ES, especially in the clinic, prudent experimental design and observations are required.

4.3. The expression changes of healing-associated growth factors induced by ES

Wound healing is a highly ordered process that requires the interaction between numerous growth factors (Barrientos *et al.*, 2008). In the present study, the result of human growth factor array assay demonstrated that several growth factors were significantly upregulated (*e.g.*, GM-CSF, PDGF, *etc.*) after 7 days of EF exposure (Lu *et al.*, 2021).

4.3.1. ES-induced GM-CSF upregulation and wound healing

GM-CSF is a glycoprotein-based growth factor synthesized by many cellular components (*e.g.*, keratinocytes, fibroblasts, *etc.*) during the wound healing process (Bussolino *et al.*, 1991, Caux *et al.*, 1992, Schirmacher *et al.*, 2001). Evidences have demonstrated that GM-CSF could increase keratinocyte migration and proliferation, thus enhancing re-epithelialization and reconstruction of the epidermal layers (Schirmacher *et al.*, 2001, Lim *et al.*, 2013, Mann *et al.*, 2006, Lu *et al.*, 2021). A study by Abedin-Do *et al.* confirmed an increased secretion of GM-CSF expressed by diabetic human skin fibroblasts after EFs exposure (Abedin-Do *et al.*, 2021), which is in agreement with our results. Besides, in some clinical studies, topical GM-CSF administration in the wound sites yielded appreciable results for the patients with chronic wounds (Bianchi *et*

al., 2002, Robson *et al.*, 2000, Payne *et al.*, 2001, Méry *et al.*, 2004), suggesting a potential therapeutic strategy to accelerate chronic wound healing via ES-induced GM-CSF upregulation (Lu *et al.*, 2021).

4.3.2. ES-induced PDGF upregulation and wound healing

In the present study, the expression of PDGF also responded to ES. Multiple cellular sources produce PDGFs, and keratinocytes are considered one of the primary sources (Bennett *et al.*, 2003, Niessen *et al.*, 2001, Uutela *et al.*, 2004). The PDGF family includes five homo- or heterodimeric subtypes (PDGF-AA, PDGF-AB, PDGF-BB, PDGF-CC, and PDGF-DD), all of which engage in the wound healing process (Bennett *et al.*, 2003, Niessen *et al.*, 2001, Uutela *et al.*, 2004). In particular, PDGFs are crucial in the angiogenesis process during wound healing, they work synergistically with vascular endothelial growth factors to increase blood vessel maturation (Stavri *et al.*, 1995). In fact, a PDGF-based medicine (recombinant human variant of PDGF-BB, becaplermin) have attained FDA approval and has been successfully applied in diabetic patients with chronic wounds (Margolis *et al.*, 2000, Margolis *et al.*, 2004). In this study, EFs exposure remarkably upregulated the PDGFs expression, this result is in agreement with the Andrew *et al*., who found the pulse EF could promote the release of PDGF in a platelet-rich plasma clot model (Frelinger III *et al.*, 2018). Meanwhile, a research by Koca Kutlu *et al.* also demonstrated that (Koca Kutlu *et al.*, 2013) transcutaneous electrical nerve stimulation could upregulate the expression of PDGF in a rat wound healing model, which provides strong supporting evidence for our study.

Since PDGFs are involved in all stages of wound healing (Uutela *et al.*, 2004), there is reason to believe this growth factor can be an efficient therapeutic target regulated by EFs for wound healing.

4.4. Involvement of ERK1/2 signaling pathway in ES-induced HaCaT cells migration

At this point, we understand that EFs can positively influence the migration, proliferation, and upregulation of the secretion of healing-associated growth

factors by keratinocytes. However, the mechanisms by which EFs initiate intracellular signaling are as yet hazy and should be additionally examined.

4.4.1. Candidate signaling pathway molecules that may respond to ES

This study selected four candidate signaling pathway molecules: ERK1/2, P38, 27HSP, and 90RSK. ERK1/2 and P38 are well-characterized subgroups of the sizeable mitogen-activated protein kinase (MAPK) family (Quintavalle *et al.*, 2011), and 90RSK (also known as $P90^{RSK}$ or MAPK-activated protein kinase-1) can be activated by the MAPK pathway (Frödin and Gammeltoft, 1999). Mounting evidence has demonstrated that the MAPK signaling pathway participates in the signal transduction of cell migration and proliferation (Yeh *et al.*, 2017, Ehnert *et al.*, 2015, Yumoto *et al.*, 2015, Sapharikas *et al.*, 2015, Manosalva *et al.*, 2020), and this was particularly the case for responding to ES or EMFs stimulation (Morotomi-Yano *et al.*, 2011, Sheikh *et al.*, 2013, McBain *et al.*, 2003). 27HSP (also known as heat shock protein 27 or heat shock protein beta-1) commonly functions as a regulator of cell development and differentiation and is also involved in signal transduction (Burban *et al.*, 2017). As a typical and regularly protective reaction, the upregulation of phospho-27HSP can fill in as a sensor of cellular stress or tissue harm (Shi *et al.*, 2003). In the present study, we focused on the changes of phosphorylation levels in ERK1/2, P38, and 90RSK, three significant members of the MAPK signaling pathway (Seger and Krebs, 1995), and as the phosphorylation changes of 27HSP (Lu *et al.*, 2021).

4.4.2. ES induce HaCaT cells response via ERK 1/2

The results of the present study demonstrated that the phosphorylation of ERK1/2 and P38 were significantly increased after the ES exposure; taking one step further, inhibition of ERK 1/2 signaling prevented the enhancement of migration by ES exposure. This indicated that the activation of the ERK 1/2 signaling cascade is essential for facilitating the effects of ES on the migration of HaCaT cells (Lu *et al.*, 2021). This comes following the results obtained by Guan *et al.*, who reported that ERK1/2 is involved in the migration of human renal tubular epithelial cells in response to physiological electric signals (Guan *et al.*, 2021).

Not only about cell migration, but multiple lines of evidence also suggest that the ERK 1/2 signaling pathway has been linked with EF-induced growth factor secretion in different cellular models. Yumoto *et al*. (Yumoto *et al.*, 2015) demonstrated that EFs upregulated PDGF and vascular endothelial growth factor expression via the ERK 1/2 and P38 pathways in osteoblastic cells. A study by Geng *et al*. (Geng *et al.*, 2019) showed evidence that ES could stimulate the secretion of fibroblast growth factor via the MAPK signaling pathway in endothelial cells, which are partially per the outcome of our findings (see Result 3.3.4.).

It is worth mentioning that, in our study, exposure to EFs did not upregulate the phosphorylation level of 27HSP, which could be regarded as no significant cellular stress being provoked by EFs with a strength of 200 mV/mm, and this is in good agreement with the results obtained by Shi *et al.* (Shi *et al.*, 2003, Lu *et al.*, 2021).

4.5. Outlook

In this study, our results revealed that EFs with a 200 mV/mm strength could accelerate wound healing *in vitro*, and all the results we obtained benefited from the newly established ES system. In future studies, a variety of cells (*e.g.*, fibroblasts, bone cells, co-culture cells, *etc.*) that respond to various ES types (*e.g.*, alternating current signal, pulse signal, *etc.*) could be investigated via the newly established ES system. Furthermore, the therapeutic effect of ES on the healing-associated pathological cell models (*e.g.*, cigarette smoke model, diabetes model, *etc.*) could also be studied and revealed. We have no doubt that we will witness the developments of ‘electrotherapy’ in the field of clinical wound healing and even tissue engineering in the near future.

5. Summary

There is developing proof that skin wound healing can be affected by external electrical fields (EFs). This study pointed toward researching the impact of EFs (200 mV/mm) on the cell migration, proliferation, and secretion of healing-associated factors of HaCaT cells (a human skin-derived cell line), as these are fundamental stages of wound healing.

We established an experimental ES system that can distribute EFs with a strength of 200V/mm to HaCaT cells, meanwhile keeping a steady cell culture climate. Compared to the works of pioneers, the newly designed system had a more straightforward structure. Moreover, it could transmit identical EF signals to up to four parallel wells, which significantly increased the reliability of the system and the reproducibility of the experiments.

The newly designed system was applied to experiments. The scratch wound closure assay was performed to evaluate HaCaT cell migration changes after exposure to EFs. Cell proliferation was assessed by calcein AM and Hoechst staining, resazurin assay, SRB staining, and DNA quantification. Expression of growth factors with the potential to assist in healing was assessed by cytokine array assay, and Western blot was performed to examine the possible signaling pathway molecules involved in responding to EF signals (Lu *et al.*, 2021).

The result showed that, after 72 h of monitoring, the pH value and temperature change in the newly designed ES system was acceptable, which means a stable cell culture environment could be kept between two medium changes (Lu *et al.*, 2021). When contrasted with the non-ES groups, the migration rate of the cells fundamentally expanded (up to 46.51%, $p < 0.05$) after 36 hours of continuous stimulation. For cell proliferation, with the application of EFs, the uptrends of the indicators above are more pronounced during the 7-day experimental period. The mitochondrial activity (up to 26.7%, $p < 0.05$), total protein content (up to 21.4%, $p < 0.05$) and total DNA content (up to 17.2%, $p < 0.05$) on day 7 in the ES groups increased significantly when compared with the non-ES groups (Lu *et al.*, 2021). The results of the cytokine array demonstrated that several growth factors were

upregulated after exposure to EFs, with significant increases in GM-CSF (up to 328.07%, $p < 0.05$) and PDGF-AB (up to 167.31%, $p < 0.05$), which are emerging as crucial players in the wound healing process and tissue reconstruction.

To further investigate the potential molecular mechanism of the response of HaCaT cells to ES, phosphorylation levels of p-ERK1/2, p-P38, p-90RSK, and p-27HSP were investigated via Western blot after 30-, 60-, 90-, and 120-min exposures to EFs, and the results showed the Western blot signals for p-ERK1/2 and p-P38 increased significantly. To confirm the role of ERK 1/2 in migration, we treated the HaCaT cells with signaling inhibitors of ERK1/2i (U0126) and P38i (SB203580), and the migration assay showed that ERK1/2i could significantly inhibit EF-induced migration. In contrast, inhibition of P38 did not show a noticeable influence on the migration of HaCaT cells, which suggested that EFs improved the migration of HaCaT cells by phosphorylating ERK1/2 signaling (Lu *et al.*, 2021).

In this study, our study demonstrates that 200 mV/mm EFs have a solid potential to accelerate wound healing by improving the migration and proliferation of keratinocytes, as well as optimizing the healing-related microenvironment, which provides an experimental basis for clinical workers to understand and apply EFs for wound healing acceleration (Lu *et al.*, 2021). Although research on mechanisms still has a long path to explore, we do not doubt that, soon, we will witness exciting developments in ‘electrotherapy’ in the field of wound healing or even tissue engineering.

6. Zusammenfassung

Es gibt immer mehr Hinweise dafür, dass das Zellverhalten durch externe elektrische Felder (EF) wesentlich beeinflusst werden kann. Es wird angenommen, dass ein Teil des Verhaltens Einfluss auf den Verlauf der Wundheilung hat. Diese Studie zielte darauf ab, die Auswirkungen von EF (200 mV/mm) auf die Zellmigration, die Proliferation und die Sekretion heilungsassoziierter Faktoren von HaCaT-Zellen (eine aus der menschlichen Haut stammende Zelllinie) zu untersuchen, da dies grundlegende Phasen der Wundheilung sind.

Wir haben ein Set-Up zur experimentellen Stimulation von HaCaT-Zellen entwickelt, mit dem elektrische Felder mit einer Stärke von 200mv/mm erzeugt und gleichmäßig an vier parallele Stimulationskammern verteilt werden konnte. Im Vergleich zu früheren Arbeiten war dieses Set-Up klarer strukturiert, wodurch die experimentelle Zuverlässigkeit und Reproduzierbarkeit deutlich erhöht werden konnte.

Zur Evaluierung der HaCaT-Zellmigration nach Exposition der EF wurde der Scratch-Wundverschlusstest durchgeführt. Die Zellproliferation wurde durch Calcein AM und Hoechst-Färbung, Resazurin-Assay, SRB-Färbung und DNA-Quantifizierung bewertet. Die Expression von potentiell heilungsunterstützenden Wachstumsfaktoren wurde mit einem Zytokin-Array-Assay evaluiert. Es wurde ein Western Blot durchgeführt, um potentielle Signalwegmoleküle zu identifizieren, die an der Reaktion auf die EF-Signale involviert sind.

Ergebnisse zeigten, dass nach einer 72 Stunden dauernden, präexperimentellen Überwachungsphase der pH-Wert und die Temperaturveränderung in des neu konzipierten Stimulations-Set-Ups zur Durchführung dieser Studien angemessen waren. Dies bedeutet, dass eine stabile Zellkulturumgebung zwischen zwei Mediumwechseln aufrechterhalten werden konnte. Im Vergleich zu den Zellkulturen, die keine Stimulation erhielten, erhöhte sich die Migrationsrate der Zellen nach 48 Stunden kontinuierlicher Stimulation grundlegend (bis zu 46,51 %, $p < 0,05$). Was den Aspekt der Zellproliferation betrifft, so sind die Aufwärtstrends der oben genannten Indikatoren bei der Anwendung von EFs während der 7-tägigen Versuchsperiode noch ausgeprägter. Die mitochondriale Aktivität (bis zu

26,7 %, $p < 0,05$), der Gesamtproteingehalt (bis zu 21,4 %, $p < 0,05$) und der Gesamt-DNA-Gehalt (bis zu 17,2 %, $p < 0,05$) stiegen am Tag 7 in den ES-Gruppen im Vergleich zu den Nicht-ES-Gruppen deutlich an.

Die Ergebnisse des Zytokin-Arrays zeigten, dass mehrere Wachstumsfaktoren nach der Exposition gegenüber EF hochreguliert wurden, mit einem signifikanten Anstieg von GM-CSF (up to 328,07%, $p < 0,05$) und PDGF-AB (up to 167,31%, $p < 0,05$), die sich als entscheidende Akteure im Wundheilungsprozess und der Geweberekonstruktion herausstellten.

Um den potenziellen molekularen Mechanismus der Reaktion von HaCaT-Zellen auf ES weiter zu untersuchen, wurden die Phosphorylierungsniveaus von p-ERK1/2, p-P38, p-90RSK und p-27HSP mittels Western Blot nach 30-, 60-, 90- und 120-minütiger Exposition gegenüber EFs untersucht Diese Ergebnisse zeigten, dass die Western Blot-Signale für p-ERK1/2 und p-P38 signifikant zunahmen. Um die Rolle von ERK 1/2 bei der Migration zu bestätigen, behandelten wir die HaCaT-Zellen mit Signalinhibitoren von ERK1/2i (U0126) und P38i (SB203580). Der Migrationstest zeigte, dass die EF-induzierte Migration durch ERK1/2i signifikant inhibiert werden konnte. Im Gegensatz dazu zeigte die Hemmung von P38 keinen offensichtlichen Einfluss auf die Migration von HaCaT-Zellen, was darauf hindeutet, dass EFs die Migration von HaCaT-Zellen durch die Phosphorylierung der ERK1/2-Signalisierung verbessert.

Unsere Studie zeigt, dass die Stimulation von Zellen mit einer elektrischen Spannung von 200 mV/mm das Potential hat, die Wundheilung aktiv zu beschleunigen, indem sie die Migration und Proliferation von Keratinozyten verbessert und die mit der Heilung zusammenhängende Mikroumgebung optimiert, was eine experimentelle Grundlage für die klinische Anwendung von EFs zur Beschleunigung der Wundheilung darstellt. Obwohl die Mechanismen weiterhin extensiv beforscht werden müssen, haben wir keinen Zweifel daran, dass wir in naher Zukunft in der "Elektrotherapie" im Bereich der Wundheilung oder sogar im Tissue Engineering weitere Anwendungsgebiete identifizieren können

7. References

ABEDIN-DO, A., ZHANG, Z., DOUVILLE, Y., MéTHOT, M. & ROUABHIA, M. 2021. Effect of electrical stimulation on diabetic human skin fibroblast growth and the secretion of cytokines and growth factors involved in wound healing. *Biology,* 10**,** 641.

AHMAD, E. T. 2008. High-voltage pulsed galvanic stimulation: effect of treatment duration on healing of chronic pressure ulcers. *Annals of Burns and Fire Disasters,* 21**,** 124.

ALLER, M.-A., ARIAS, J.-I. & ARIAS, J. 2010. Pathological axes of wound repair: gastrulation revisited. *Theoretical Biology and Medical Modelling,* 7**,** 1-32.

AMBIC, H., REYES, E., MANNING, T., WATERS, K. & REGER, S. 1993. Influence of AC and DC electrical stimulation on wound healing in pigs: a biomechanical analysis. *Journal of Investigative Surgery,* 6**,** 535-543.

ANDERSON, L., LEUNG, F., ROMMEREIM, D., BUSCHBOM, R., WILSON, B. & STEVENS, R. 1989. Effect of chronic 60-Hz electric field exposure on mammary tumorigenesis in the rat. Pacific Northwest National Lab.(PNNL), Richland, WA (United States).

ARAGóN, Á., CEBRO-MáRQUEZ, M., PEREZ, E., PAZOS, A., LAGE, R., GONZáLEZ-JUANATEY, J. R., MOSCOSO, I., BAO-VARELA, C. & NIETO, D. 2020. Bioelectronics-on-a-chip for cardio myoblast proliferation enhancement using electric field stimulation. *Biomaterials Research,* 24**,** 1-10.

ASPERA-WERZ, R. H., EHNERT, S., MüLLER, M., ZHU, S., CHEN, T., WENG, W., JACOBY, J. & NUSSLER, A. K. 2020. Assessment of tobacco heating system 2.4 on osteogenic differentiation of mesenchymal stem cells and primary human osteoblasts compared to conventional cigarettes. *World Journal of Stem Cells,* 12**,** 841.

AU, H. T. H., CHENG, I., CHOWDHURY, M. F. & RADISIC, M. 2007. Interactive effects of surface topography and pulsatile electrical field stimulation on orientation and elongation of fibroblasts and cardiomyocytes. *Biomaterials,* 28**,** 4277-4293.

BALINT, R., CASSIDY, N. J. & CARTMELL, S. H. 2013. Electrical stimulation: a novel tool for tissue engineering. *Tissue Engineering Part B: Reviews,* 19**,** 48-57.

BARKER, A., JAFFE, L. & VANABLE JR, J. 1982. The glabrous epidermis of cavies contains a powerful battery. *American Journal of Physiology-Regulatory, Integrative and Comparative Physiology,* 242**,** R358-R366.

BARRIENTOS, S., STOJADINOVIC, O., GOLINKO, M. S., BREM, H. & TOMIC-CANIC, M. 2008. Growth factors and cytokines in wound healing. *Wound repair and regeneration,* 16**,** 585-601.

BENNETT, S., GRIFFITHS, G., SCHOR, A., LEESE, G. & SCHOR, S. 2003. Growth factors in the treatment of diabetic foot ulcers. *Journal of British Surgery,* 90**,** 133-146.

BIANCHI, L., GINEBRI, A., HAGMAN, J., FRANCESCONI, F., CARBONI, I. & CHIMENTI, S. 2002. Local treatment of chronic cutaneous leg ulcers with recombinant human granulocyte-macrophage colony-stimulating factor. *Journal of the European Academy of Dermatology and Venereology,* 16**,** 595-598.

BJöRNINEN, M., GILMORE, K., PELTO, J., SEPPäNEN-KAIJANSINKKO, R., KELLOMäKI, M., MIETTINEN, S., WALLACE, G., GRIJPMA, D. & HAIMI, S. 2017. Electrically stimulated adipose stem cells on polypyrrole-coated scaffolds for smooth muscle tissue engineering. *Annals of biomedical engineering,* 45**,** 1015-1026.

BLACHE, U. & EHRBAR, M. 2018. Inspired by nature: hydrogels as versatile tools for

vascular engineering. *Advances in wound care,* 7**,** 232-246.
BUCEKOVA, M., SOJKA, M., VALACHOVA, I., MARTINOTTI, S., RANZATO, E., SZEP, Z., MAJTAN, V., KLAUDINY, J. & MAJTAN, J. 2017. Bee-derived antibacterial peptide, defensin-1, promotes wound reepithelialisation in vitro and in vivo. *Wound Healing Southern Africa,* 10**,** 25-35.
BURBAN, A., SHARANEK, A., HüE, R., GAY, M., ROUTIER, S., GUILLOUZO, A. & GUGUEN-GUILLOUZO, C. 2017. Penicillinase-resistant antibiotics induce non-immune-mediated cholestasis through HSP27 activation associated with PKC/P38 and PI3K/AKT signaling pathways. *Scientific reports,* 7**,** 1-17.
BUSSOLINO, F., ZICHE, M., WANG, J. M., ALESSI, D., MORBIDELLI, L., CREMONA, O., BOSIA, A., MARCHISIO, P. C. & MANTOVANI, A. 1991. In vitro and in vivo activation of endothelial cells by colony-stimulating factors. *The Journal of clinical investigation,* 87**,** 986-995.
CANCEDDA, R., BOLLINI, S., DESCALZI, F., MASTROGIACOMO, M. & TASSO, R. 2017. Learning from mother nature: innovative tools to boost endogenous repair of critical or difficult-to-heal large tissue defects. *Frontiers in bioengineering and biotechnology,* 5**,** 28.
CARROLL, D., MOORE, R., MCQUAY, H. H., FAIRMAN, F. S., TRAMèR, M., LEIJON, G. G. & MOORE, A. 2000. Transcutaneous electrical nerve stimulation (TENS) for chronic pain. *Cochrane Database of Systematic Reviews*.
CAUX, C., DEZUTTER-DAMBUYANT, C., SCHMITT, D. & BANCHEREAU, J. 1992. GM-CSF and TNF-α cooperate in the generation of dendritic Langerhans cells. *Nature,* 360**,** 258-261.
CHAMCHEU, J. C., ROY, T., UDDIN, M. B., BANANG-MBEUMI, S., CHAMCHEU, R.-C. N., WALKER, A. L., LIU, Y.-Y. & HUANG, S. 2019. Role and therapeutic targeting of the PI3K/Akt/mTOR signaling pathway in skin cancer: a review of current status and future trends on natural and synthetic agents therapy. *Cells,* 8**,** 803.
CHAMCHEU, J. C., SIDDIQUI, I. A., SYED, D. N., ADHAMI, V. M., LIOVIC, M. & MUKHTAR, H. 2011. Keratin gene mutations in disorders of human skin and its appendages. *Archives of biochemistry and biophysics,* 508**,** 123-137.
CHEN, Y., ASPERA-WERZ, R. H., MENGER, M. M., FALLDORF, K., RONNIGER, M., STACKE, C., HISTING, T., NUSSLER, A. K. & EHNERT, S. 2021. Exposure to 16 Hz Pulsed Electromagnetic Fields Protect the Structural Integrity of Primary Cilia and Associated TGF-β Signaling in Osteoprogenitor Cells Harmed by Cigarette Smoke. *International journal of molecular sciences,* 22**,** 7036.
CHO, Y., SON, M., JEONG, H. & SHIN, J. H. 2018. Electric field–induced migration and intercellular stress alignment in a collective epithelial monolayer. *Molecular biology of the cell,* 29**,** 2292-2302.
CUI, S., ROUABHIA, M., SEMLALI, A. & ZHANG, Z. 2021. Effects of electrical stimulation on human skin keratinocyte growth and the secretion of cytokines and growth factors. *Biomedical Materials,* 16**,** 065021.
DORSCHNER, R. A., LEE, J., COHEN, O., COSTANTINI, T., BAIRD, A. & ELICEIRI, B. P. 2020. ECRG4 regulates neutrophil recruitment and CD44 expression during the inflammatory response to injury. *Science advances,* 6**,** eaay0518.
DUNN, M. G., DOILLON, C. J., BERG, R. A., OLSON, R. M. & SILVER, F. H. 1988. Wound healing using a collagen matrix: effect of DC electrical stimulation. *Journal of biomedical materials research,* 22**,** 191-206.
EDWICK, D. O., HINCE, D. A., RAWLINS, J. M., WOOD, F. M. & EDGAR, D. W. 2022. Does electrical stimulation improve healing in acute minor burn injury, as measured by bioimpedance spectroscopy? A single center, randomized, controlled trial. *Burns Open,* 6**,** 42-50.
EHNERT, S., ASPERA-WERZ, R. H., IHLE, C., TROST, M., ZIRN, B., FLESCH, I.,

SCHRöTER, S., RELJA, B. & NUSSLER, A. K. 2019a. Smoking dependent alterations in bone formation and inflammation represent major risk factors for complications following total joint arthroplasty. *Journal of clinical medicine,* 8**,** 406.

EHNERT, S., FALLDORF, K., FENTZ, A.-K., ZIEGLER, P., SCHRöTER, S., FREUDE, T., OCHS, B. G., STACKE, C., RONNIGER, M. & SACHTLEBEN, J. 2015. Primary human osteoblasts with reduced alkaline phosphatase and matrix mineralization baseline capacity are responsive to extremely low frequency pulsed electromagnetic field exposure—Clinical implication possible. *Bone Reports,* 3**,** 48-56.

EHNERT, S., LINNEMANN, C., ASPERA-WERZ, R. H., BYKOVA, D., BIERMANN, S., FECHT, L., DE ZWART, P. M., NUSSLER, A. K. & STUBY, F. 2018a. Immune cell induced migration of osteoprogenitor cells is mediated by TGF-β dependent upregulation of NOX4 and activation of focal adhesion kinase. *International journal of molecular sciences,* 19**,** 2239.

EHNERT, S., LINNEMANN, C., BRAUN, B., BOTSCH, J., LEIBIGER, K., HEMMANN, P. & NUSSLER, A. K. 2019b. One-Step ARMS-PCR for the Detection of SNPs—Using the example of the PADI4 Gene. *Methods and protocols,* 2**,** 63.

EHNERT, S., VAN GRIENSVEN, M., UNGER, M., SCHEFFLER, H., FALLDORF, K., FENTZ, A.-K., SEELIGER, C., SCHRöTER, S., NUSSLER, A. K. & BALMAYOR, E. R. 2018b. Co-culture with human osteoblasts and exposure to extremely low frequency pulsed electromagnetic fields improve osteogenic differentiation of human adipose-derived mesenchymal stem cells. *International journal of molecular sciences,* 19**,** 994.

EMING, S. A., HAMMERSCHMIDT, M., KRIEG, T. & ROERS, A. Interrelation of immunity and tissue repair or regeneration. Seminars in cell & developmental biology, 2009. Elsevier, 517-527.

EMING, S. A., KRIEG, T. & DAVIDSON, J. M. 2007. Inflammation in wound repair: molecular and cellular mechanisms. *Journal of Investigative Dermatology,* 127**,** 514-525.

ERCAN, B. & WEBSTER, T. J. 2010. The effect of biphasic electrical stimulation on osteoblast function at anodized nanotubular titanium surfaces. *Biomaterials,* 31**,** 3684-3693.

FEDROWITZ, M. & LöSCHER, W. 2008. Exposure of Fischer 344 rats to a weak power frequency magnetic field facilitates mammary tumorigenesis in the DMBA model of breast cancer. *Carcinogenesis,* 29**,** 186-193.

FORE, J. 2006. A review of skin and the effects of aging on skin structure and function. *Ostomy/wound management,* 52**,** 24-35; quiz 36.

FOULDS, I. & BARKER, A. 1983. Human skin battery potentials and their possible role in wound healing. *British Journal of Dermatology,* 109**,** 515-522.

FRANKLIN, B. M., MAROUDAS, E. & OSBORN, J. L. 2016. Sine-wave electrical stimulation initiates a voltage-gated potassium channel-dependent soft tissue response characterized by induction of hemocyte recruitment and collagen deposition. *Physiological reports,* 4**,** e12832.

FRELINGER III, A. L., GERRITS, A. J., NECULAES, V. B., GREMMEL, T., TORRES, A. S., CAIAFA, A., CARMICHAEL, S. L. & MICHELSON, A. D. 2018. Tunable activation of therapeutic platelet-rich plasma by pulse electric field: Differential effects on clot formation, growth factor release, and platelet morphology. *Plos one,* 13**,** e0203557.

FRöDIN, M. & GAMMELTOFT, S. 1999. Role and regulation of 90 kDa ribosomal S6 kinase (RSK) in signal transduction. *Molecular and cellular endocrinology,* 151**,** 65-77.

GENG, K., WANG, J., LIU, P., TIAN, X., LIU, H., WANG, X., HU, C. & YAN, H. 2019. Electrical stimulation facilitates the angiogenesis of human umbilical vein endothelial cells through MAPK/ERK signaling pathway by stimulating FGF2 secretion. *American Journal of Physiology-Cell Physiology,* 317**,** C277-C286.

GILABERTE, Y., PRIETO-TORRES, L., PASTUSHENKO, I. & JUARRANZ, Á. 2016. Anatomy and Function of the Skin. *Nanoscience in Dermatology.* Elsevier.

GOLDMAN, R. & POLLACK, S. 1996. Electric fields and proliferation in a chronic wound model. *Bioelectromagnetics: Journal of the Bioelectromagnetics Society, The Society for Physical Regulation in Biology and Medicine, The European Bioelectromagnetics Association,* 17**,** 450-457.

GONZALEZ, A. C. D. O., COSTA, T. F., ANDRADE, Z. D. A. & MEDRADO, A. R. A. P. 2016. Wound healing-A literature review. *Anais brasileiros de dermatologia,* 91**,** 614-620.

GRAINGER, A. 2014. *The Characterization of Enhancer Elements Involved in the Spatial Patterning of the Skin.* UC San Diego.

GUAN, L., FAN, P., LIU, X., LIU, R., LIU, Y. & BAI, H. 2021. Migration of Human Renal Tubular Epithelial Cells in Response to Physiological Electric Signals. *Frontiers in Cell and Developmental Biology,* 9.

GURTNER, G. C., WERNER, S., BARRANDON, Y. & LONGAKER, M. T. 2008. Wound repair and regeneration. *Nature,* 453**,** 314-321.

HAMBURGER, V. 1942. *A manual of experimental embryology*, The University of Chicago Press.

HANDLY, L. N. & WOLLMAN, R. 2017. Wound-induced Ca2+ wave propagates through a simple release and diffusion mechanism. *Molecular biology of the cell,* 28**,** 1457-1466.

HANG, J., KONG, L., GU, J. & ADAIR, T. 1995. VEGF gene expression is upregulated in electrically stimulated rat skeletal muscle. *American Journal of Physiology-Heart and Circulatory Physiology,* 269**,** H1827-H1831.

HARRISON-BALESTRA, C., CAZZANIGA, A. L., DAVIS, S. C. & MERTZ, P. M. 2003. A wound-isolated Pseudomonas aeruginosa grows a biofilm in vitro within 10 hours and is visualized by light microscopy. *Dermatologic surgery,* 29**,** 631-635.

HENRIKSEN, J. L., SøRENSEN, N. B., FINK, T., ZACHAR, V. & PORSBORG, S. R. 2020. Systematic Review of Stem-Cell-Based Therapy of Burn Wounds: Lessons Learned from Animal and Clinical Studies. *Cells,* 9**,** 2545.

JAFFE, L. F. & VANABLE JR, J. W. 1984. Electric fields and wound healing. *Clinics in dermatology,* 2**,** 34-44.

JI, R., TENG, M., ZHANG, Z., WANG, W., ZHANG, Q., LV, Y., ZHANG, J. & JIANG, X. 2020. Electric field down-regulates CD9 to promote keratinocytes migration through AMPK pathway. *International journal of medical sciences,* 17**,** 865.

KALAILINGAM, P., TAN, H. B., PAN, J. Y., TAN, S. H. & THANABALU, T. 2019. Overexpression of CDC42SE1 in A431 cells reduced cell proliferation by inhibiting the Akt pathway. *Cells,* 8**,** 117.

KEMPPAINEN, P., LEPPäNEN, H., JYVäSJäRVI, E. & PERTOVAARA, A. 1994. Blood flow increase in the orofacial area of humans induced by painful stimulation. *Brain research bulletin,* 33**,** 655-662.

KIM, I. S., SONG, J. K., SONG, Y. M., CHO, T. H., LEE, T. H., LIM, S. S., KIM, S. J. & HWANG, S. J. 2009. Novel effect of biphasic electric current on in vitro osteogenesis and cytokine production in human mesenchymal stromal cells. *Tissue Engineering Part A,* 15**,** 2411-2422.

KIRSON, E. D., GURVICH, Z., SCHNEIDERMAN, R., DEKEL, E., ITZHAKI, A., WASSERMAN, Y., SCHATZBERGER, R. & PALTI, Y. 2004. Disruption of cancer

cell replication by alternating electric fields. *Cancer research,* 64**,** 3288-3295.
KLOTH, L. C. 2014. Electrical stimulation technologies for wound healing. *Advances in wound care,* 3**,** 81-90.
KOCA KUTLU, A., ÇEçEN, D., GüRGEN, S. G., SAYıN, O. & ÇETIN, F. 2013. A comparison study of growth factor expression following treatment with transcutaneous electrical nerve stimulation, saline solution, povidone-iodine, and lavender oil in wounds healing. *Evidence-Based Complementary and Alternative Medicine,* 2013.
KOPPES, A. N., SEGGIO, A. M. & THOMPSON, D. M. 2011. Neurite outgrowth is significantly increased by the simultaneous presentation of Schwann cells and moderate exogenous electric fields. *Journal of neural engineering,* 8**,** 046023.
KWON, H., KIM, D. & KIM, J. S. 2017. Body fat distribution and the risk of incident metabolic syndrome: a longitudinal cohort study. *Scientific reports,* 7**,** 1-8.
LABAT-ROBERT, J. 2012. Information exchanges between cells and extracellular matrix. Influence of aging. *Biologie aujourd'hui,* 206**,** 103-109.
LEVIN, M. 2007. Large-scale biophysics: ion flows and regeneration. *Trends in cell biology,* 17**,** 261-270.
LEVIN, M. H., KIM, J. K., HU, J. & VERKMAN, A. 2006. Potential difference measurements of ocular surface Na+ absorption analyzed using an electrokinetic model. *Investigative ophthalmology & visual science,* 47**,** 306-316.
LEVIN, M. H. & VERKMAN, A. 2005. CFTR-regulated chloride transport at the ocular surface in living mice measured by potential differences. *Investigative ophthalmology & visual science,* 46**,** 1428-1434.
LIANG, C.-C., PARK, A. Y. & GUAN, J.-L. 2007. In vitro scratch assay: a convenient and inexpensive method for analysis of cell migration in vitro. *Nature protocols,* 2**,** 329-333.
LIM, J.-Y., CHOI, B. H., LEE, S., JANG, Y. H., CHOI, J.-S. & KIM, Y.-M. 2013. Regulation of wound healing by granulocyte-macrophage colony-stimulating factor after vocal fold injury. *PloS one,* 8**,** e54256.
LOWRY, O. H., ROSEBROUGH, N. J., FARR, A. L. & RANDALL, R. J. 1951. Protein measurement with the Folin phenol reagent. *Journal of biological chemistry,* 193**,** 265-275.
LU, C., KOLBENSCHLAG, J., NüSSLER, A. K., EHNERT, S., MCCAIG, C. D., ČEBRON, U., DAIGELER, A. & PRAHM, C. 2021. Direct Current Electrical Fields Improve Experimental Wound Healing by Activation of Cytokine Secretion and Erk1/2 Pathway Stimulation. *Life,* 11**,** 1195.
LUO, R., DAI, J., ZHANG, J. & LI, Z. 2021a. Accelerated skin wound healing by electrical stimulation. *Advanced Healthcare Materials,* 10**,** 2100557.
LUO, R., DAI, J., ZHANG, J. & LI, Z. 2021b. Accelerated Skin Wound Healing by Electrical Stimulation. *Advanced Healthcare Materials***,** 2100557.
MAHMOUD, N., AL-KHARABSHEH, L., KHALIL, E. & ABU-DAHAB, R. 2019. Interaction of gold nanorods with human dermal fibroblasts: cytotoxicity. *Cellular Uptake, and Wound Healing, Nanomater.(Basel, Switzerland),* 9.
MANN, A., NIEKISCH, K., SCHIRMACHER, P. & BLESSING, M. Granulocyte–macrophage colony-stimulating factor is essential for normal wound healing. Journal of Investigative Dermatology Symposium Proceedings, 2006. Elsevier, 87-92.
MANOSALVA, C., ALARCóN, P., GONZáLEZ, K., SOTO, J., IGOR, K., PEñA, F., MEDINA, G., BURGOS, R. A. & HIDALGO, M. A. 2020. Free fatty acid receptor 1 signaling contributes to migration, MMP-9 activity, and expression of IL-8 induced by linoleic acid in HaCaT cells. *Frontiers in Pharmacology,* 11**,** 595.
MARGOLIS, D. J., CROMBLEHOLME, T. & HERLYN, M. 2000. Clinical Protocol: Phase

I trial to evaluate the safety of H5. 020CMV. PDGF‐B for the treatment of a diabetic insensate foot ulcer. *Wound repair and regeneration,* 8**,** 480-493.
MARGOLIS, D. J., CROMBLEHOME, T., HERLYN, M., CROSS, P., WEINBERG, L., FILIP, J. & PROPERT, K. 2004. Phase I trial to evaluate the safety of H5. 020CMV. PDGF-B and limb compression bandage for the treatment of venous leg ulcer: trial A. *Human gene therapy,* 15**,** 1003-1019.
MCBAIN, V. A., FORRESTER, J. V. & MCCAIG, C. D. 2003. HGF, MAPK, and a small physiological electric field interact during corneal epithelial cell migration. *Investigative ophthalmology & visual science,* 44**,** 540-547.
MCCAIG, C. 2008. Electrical control of cell behaviour and wound healing. *GMS Krankenhaushygiene interdisziplinar,* 3.
MCCAIG, C. D., ALLAN, D., ERSKINE, L., RAJNICEK, A. M. & STEWART, R. 1994. Growing nerves in an electric field. *Neuroprotocols,* 4**,** 134-141.
MCCAIG, C. D., RAJNICEK, A. M., SONG, B. & ZHAO, M. 2005. Controlling cell behavior electrically: current views and future potential. *Physiological reviews*.
MEEKER, N. D., HUTCHINSON, S. A., HO, L. & TREDE, N. S. 2007. Method for isolation of PCR-ready genomic DNA from zebrafish tissues. *Biotechniques,* 43**,** 610-614.
MERRILL, D. R., BIKSON, M. & JEFFERYS, J. G. 2005. Electrical stimulation of excitable tissue: design of efficacious and safe protocols. *Journal of neuroscience methods,* 141**,** 171-198.
MéRY, L., GIROT, R. & ARACTINGI, S. 2004. Topical effectiveness of molgramostim (GM-CSF) in sickle cell leg ulcers. *Dermatology,* 208**,** 135-137.
MOROTOMI-YANO, K., AKIYAMA, H. & YANO, K.-I. 2011. Nanosecond pulsed electric fields activate MAPK pathways in human cells. *Archives of biochemistry and biophysics,* 515**,** 99-106.
NIESSEN, F. B., ANDRIESSEN, M. P., SCHALKWIJK, J., VISSER, L. & TIMENS, W. 2001. Keratinocyte‐derived growth factors play a role in the formation of hypertrophic scars. *The Journal of Pathology: A Journal of the Pathological Society of Great Britain and Ireland,* 194**,** 207-216.
NIKITKINA, A. I., BIKMULINA, P. Y., GAFAROVA, E. R., KOSHELEVA, N. V., EFREMOV, Y. M., BEZRUKOV, E. A., BUTNARU, D. V., DOLGANOVA, I. N., CHERNOMYRDIN, N. V. & CHERKASOVA, O. P. 2021. Terahertz radiation and the skin: a review. *Journal of Biomedical Optics,* 26**,** 043005.
NISHIMURA, K. Y., ISSEROFF, R. R. & NUCCITELLI, R. 1996. Human keratinocytes migrate to the negative pole in direct current electric fields comparable to those measured in mammalian wounds. *Journal of cell science,* 109**,** 199-207.
PAYNE, W. G., OCHS, D. E., MELTZER, D. D., HILL, D. P., MANNARI, R. J., ROBSON, L. E. & ROBSON, M. C. 2001. Long-term outcome study of growth factor-treated pressure ulcers. *The American journal of surgery,* 181**,** 81-86.
PELLETIER, S. J., LAGACé, M., ST-AMOUR, I., ARSENAULT, D., CISBANI, G., CHABRAT, A., FECTEAU, S., LéVESQUE, M. & CICCHETTI, F. 2015. The morphological and molecular changes of brain cells exposed to direct current electric field stimulation. *International Journal of Neuropsychopharmacology,* 18.
POLAK, A., KLOTH, L. C., BLASZCZAK, E., TARADAJ, J., NAWRAT-SZOLTYSIK, A., ICKOWICZ, T., HORDYNSKA, E., FRANEK, A. & KUCIO, C. 2017. The efficacy of pressure ulcer treatment with cathodal and cathodal-anodal high-voltage monophasic pulsed current: a prospective, randomized, controlled clinical trial. *Physical therapy,* 97**,** 777-789.
POLAK, A., TARADAJ, J., NAWRAT-SZOLTYSIK, A., STANIA, M., DOLIBOG, P., BLASZCZAK, E., ZARZECZNY, R., JURAS, G., FRANEK, A. & KUCIO, C. 2016. Reduction of pressure ulcer size with high-voltage pulsed current and high-

frequency ultrasound: a randomised trial. *Journal of wound care,* 25**,** 742-754.
QUAN, T. & FISHER, G. J. 2015. Role of age-associated alterations of the dermal extracellular matrix microenvironment in human skin aging: a mini-review. *Gerontology,* 61**,** 427-434.
QUARESMA, J. A. S. 2019. Organization of the skin immune system and compartmentalized immune responses in infectious diseases. *Clinical microbiology reviews,* 32**,** e00034-18.
QUINTAVALLE, C., BRENCA, M., DE MICCO, F., FIORE, D., ROMANO, S., ROMANO, M., APONE, F., BIANCO, A., ZABATTA, M. & TRONCONE, G. 2011. In vivo and in vitro assessment of pathways involved in contrast media-induced renal cells apoptosis. *Cell death & disease,* 2**,** e155-e155.
RAJNICEK, A. M., STUMP, R. F. & ROBINSON, K. R. 1988. An endogenous sodium current may mediate wound healing in Xenopus neurulae. *Developmental biology,* 128**,** 290-299.
RAJNICEK, A. M., ZHAO, Z., MORAL‐VICO, J., CRUZ, A. M., MCCAIG, C. D. & CASAñ‐PASTOR, N. 2018. Controlling nerve growth with an electric field induced indirectly in transparent conductive substrate materials. *Advanced Healthcare Materials,* 7**,** 1800473.
ROBSON, M. C., HILL, D. P., SMITH, P. D., WANG, X., MEYER-SIEGLER, K., KO, F., VANDEBERG, J. S., PAYNE, W. G., OCHS, D. & ROBSON, L. E. 2000. Sequential cytokine therapy for pressure ulcers: clinical and mechanistic response. *Annals of surgery,* 231**,** 600.
RODRIGUES, M., KOSARIC, N., BONHAM, C. A. & GURTNER, G. C. 2019. Wound healing: a cellular perspective. *Physiological reviews,* 99**,** 665-706.
SANTORO, M. M. & GAUDINO, G. 2005. Cellular and molecular facets of keratinocyte reepithelization during wound healing. *Experimental cell research,* 304**,** 274-286.
SAPHARIKAS, E., LOKAJCZYK, A., FISCHER, A.-M. & BOISSON-VIDAL, C. 2015. Fucoidan stimulates Monocyte migration via ERK/p38 signaling pathways and MMP9 secretion. *Marine drugs,* 13**,** 4156-4170.
SAUER, H., BEKHITE, M. M., HESCHELER, J. & WARTENBERG, M. 2005. Redox control of angiogenic factors and CD31-positive vessel-like structures in mouse embryonic stem cells after direct current electrical field stimulation. *Experimental cell research,* 304**,** 380-390.
SCHäFER, M. & WERNER, S. 2008. Cancer as an overhealing wound: an old hypothesis revisited. *Nature reviews Molecular cell biology,* 9**,** 628-638.
SCHIRMACHER, P., MANN, A., BREUHAHN, K. & BLESSING, M. 2001. Keratinocyte-derived granulocyte-macrophage colony stimulating factor accelerates wound healing: stimulation of keratinocyte proliferation, granulation tissue formation, and vascularization. *Journal of Investigative Dermatology,* 117**,** 1382-1390.
SCHMITZ, G., ROSENBLATT, L., SALERNO, N., ODETTE, J., REN, R., EMANUEL, T., MICHALEK, J., LIU, Q., DU, L. & JAHANGIR, K. 2019. Treatment data using a topical povidone-iodine antiseptic in patients with superficial skin abscesses. *Data in brief,* 23**,** 103715.
SCHOOP, V. M., FUSENIG, N. E. & MIRANCEA, N. 1999. Epidermal organization and differentiation of HaCaT keratinocytes in organotypic coculture with human dermal fibroblasts. *Journal of investigative dermatology,* 112**,** 343-353.
SEGER, R. & KREBS, E. G. 1995. The MAPK signaling cascade. *The FASEB journal,* 9**,** 726-735.
SEO, B. F. & JUNG, S.-N. 2016. The immunomodulatory effects of mesenchymal stem cells in prevention or treatment of excessive scars. *Stem cells international,* 2016.
SHAPIRO, S., BORGENS, R., PASCUZZI, R., ROOS, K., GROFF, M., PURVINES, S., RODGERS, R. B., HAGY, S. & NELSON, P. 2005. Oscillating field stimulation for

complete spinal cord injury in humans: a phase 1 trial. *Journal of Neurosurgery: spine,* 2**,** 3-10.
SHEIKH, A. Q., TAGHIAN, T., HEMINGWAY, B., CHO, H., KOGAN, A. B. & NARMONEVA, D. A. 2013. Regulation of endothelial MAPK/ERK signalling and capillary morphogenesis by low-amplitude electric field. *Journal of the Royal Society Interface,* 10**,** 20120548.
SHI, B., FARBOUD, B., NUCCITELLI, R. & ISSEROFF, R. R. 2003. Power-line frequency electromagnetic fields do not induce changes in phosphorylation, localization, or expression of the 27-kilodalton heat shock protein in human keratinocytes. *Environmental health perspectives,* 111**,** 281-288.
SKEHAN, P., STORENG, R., SCUDIERO, D., MONKS, A., MCMAHON, J., VISTICA, D., WARREN, J. T., BOKESCH, H., KENNEY, S. & BOYD, M. R. 1990. New colorimetric cytotoxicity assay for anticancer-drug screening. *JNCI: Journal of the National Cancer Institute,* 82**,** 1107-1112.
SOIB, H. H., ISMAIL, H. F., HUSIN, F., ABU BAKAR, M. H., YAAKOB, H. & SARMIDI, M. R. 2020. Bioassay-guided different extraction techniques of Carica papaya (Linn.) leaves on in vitro wound-healing activities. *Molecules,* 25**,** 517.
SONG, B., GU, Y., PU, J., REID, B., ZHAO, Z. & ZHAO, M. 2007. Application of direct current electric fields to cells and tissues in vitro and modulation of wound electric field in vivo. *Nature protocols,* 2**,** 1479-1489.
SPADARO, J. & BECKER, R. 1979. Function of implanted cathodes in electrode-induced bone growth. *Medical and Biological Engineering and Computing,* 17**,** 769-775.
STAVRI, G. T., HONG, Y., ZACHARY, I. C., BREIER, G., BASKERVILLE, P. A., YLä-HERTTUALA, S., RISAU, W., MARTIN, J. F. & ERUSALIMSKY, J. D. 1995. Hypoxia and platelet-derived growth factor-BB synergistically upregulate the expression of vascular endothelial growth factor in vascular smooth muscle cells. *Febs Letters,* 358**,** 311-315.
STRECKER-MCGRAW, M. K., JONES, T. R. & BAER, D. G. 2007. Soft tissue wounds and principles of healing. *Emergency medicine clinics of North America,* 25**,** 1-22.
SZABOWSKI, A., MAAS-SZABOWSKI, N., ANDRECHT, S., KOLBUS, A., SCHORPP-KISTNER, M., FUSENIG, N. E. & ANGEL, P. 2000. c-Jun and JunB antagonistically control cytokine-regulated mesenchymal–epidermal interaction in skin. *Cell,* 103**,** 745-755.
TANDON, N., CANNIZZARO, C., CHAO, P.-H. G., MAIDHOF, R., MARSANO, A., AU, H. T. H., RADISIC, M. & VUNJAK-NOVAKOVIC, G. 2009. Electrical stimulation systems for cardiac tissue engineering. *Nature protocols,* 4**,** 155-173.
THAWER, H. A. & HOUGHTON, P. E. 2001. Effects of electrical stimulation on the histological properties of wounds in diabetic mice. *Wound Repair and Regeneration,* 9**,** 107-115.
TITUSHKIN, I. & CHO, M. 2009. Regulation of cell cytoskeleton and membrane mechanics by electric field: role of linker proteins. *Biophysical journal,* 96**,** 717-728.
TONNESEN, M. G., FENG, X. & CLARK, R. A. Angiogenesis in wound healing. Journal of Investigative Dermatology Symposium Proceedings, 2000. Elsevier, 40-46.
UD-DIN, S. & BAYAT, A. Electrical stimulation and cutaneous wound healing: a review of clinical evidence. Healthcare, 2014. Multidisciplinary Digital Publishing Institute, 445-467.
USUI, M. L., MANSBRIDGE, J. N., CARTER, W. G., FUJITA, M. & OLERUD, J. E. 2008. Keratinocyte migration, proliferation, and differentiation in chronic ulcers from patients with diabetes and normal wounds. *Journal of Histochemistry & Cytochemistry,* 56**,** 687-696.
UUTELA, M., WIRZENIUS, M., PAAVONEN, K., RAJANTIE, I., HE, Y., KARPANEN, T.,

LOHELA, M., WIIG, H., SALVEN, P. & PAJUSOLA, K. 2004. PDGF-D induces macrophage recruitment, increased interstitial pressure, and blood vessel maturation during angiogenesis. *Blood,* 104**,** 3198-3204.

VADLAMANI, R. A., NIE, Y., DETWILER, D. A., DHANABAL, A., KRAFT, A. M., KUANG, S., GAVIN, T. P. & GARNER, A. L. 2019. Nanosecond pulsed electric field induced proliferation and differentiation of osteoblasts and myoblasts. *Journal of the Royal Society Interface,* 16**,** 20190079.

WALMSLEY, G. G., MAAN, Z. N., WONG, V. W., DUSCHER, D., HU, M. S., ZIELINS, E. R., WEARDA, T., MUHONEN, E., MCARDLE, A. & TEVLIN, R. 2015. Scarless wound healing: chasing the holy grail. *Plastic and reconstructive surgery,* 135**,** 907-917.

WANG, Z., EHNERT, S., IHLE, C., SCHYSCHKA, L., PSCHERER, S., NUSSLER, N. C., BRAUN, K. F., VAN GRIENSVEN, M., WANG, G. & BURGKART, R. 2014. Increased oxidative stress response in granulocytes from older patients with a hip fracture may account for slow regeneration. *Oxidative medicine and cellular longevity,* 2014.

WEISS, D. S., EAGLSTEIN, W. H. & FALANGA, V. 1989. Exogenous electric current can reduce the formation of hypertrophic scars. *The Journal of dermatologic surgery and oncology,* 15**,** 1272-1276.

WOLCOTT, L., WHEELER, P., HARDWICKE, H. & ROWLEY, B. 1969. Accelerated healing of skin ulcers by electrotherapy: preliminary clinical results. *Southern medical journal,* 62**,** 795-801.

WON, H.-R., SEO, C., LEE, H.-Y., ROH, J., KIM, C.-H., JANG, J. Y. & SHIN, Y. S. 2019. An important role of macrophages for wound margin regeneration in a murine flap model. *Tissue engineering and regenerative medicine,* 16**,** 667-674.

WONGA, K. W. & MAHA, S. H. 2021. A review on xanthone derivatives with antiinflammatory effects and their structure–activity relationship. *Studies in Natural Products Chemistry***,** 10393.

XIA, Y., CHEN, J., DING, J., ZHANG, J. & CHEN, H. 2020. IGF1-and BM-MSC-incorporating collagen-chitosan scaffolds promote wound healing and hair follicle regeneration. *American Journal of Translational Research,* 12**,** 6264.

YARON, J. R., ZHANG, L., GUO, Q., AWO, E. A., BURGIN, M., SCHUTZ, L. N., ZHANG, N., KILBOURNE, J., DAGGETT-VONDRAS, J. & LOWE, K. M. 2020. Recombinant myxoma virus-derived immune modulator M-T7 accelerates cutaneous wound healing and improves tissue remodeling. *Pharmaceutics,* 12**,** 1003.

YEH, C.-J., CHEN, C.-C., LEU, Y.-L., LIN, M.-W., CHIU, M.-M. & WANG, S.-H. 2017. The effects of artocarpin on wound healing: in vitro and in vivo studies. *Scientific reports,* 7**,** 1-13.

YUMOTO, H., HIRAO, K., TOMINAGA, T., BANDO, N., TAKAHASHI, K. & MATSUO, T. 2015. Electromagnetic wave irradiation promotes osteoblastic cell proliferation and up-regulates growth factors via activation of the ERK1/2 and p38 MAPK pathways. *Cellular Physiology and Biochemistry,* 35**,** 601-615.

ZAMORA-NAVAS, P., AYUSO JR, S. & REINA, P. 1995. Electrical stimulation of bone nonunion with the presence of a gap. *Acta orthopaedica belgica,* 61**,** 169-176.

ZHAO, M. Electrical fields in wound healing—an overriding signal that directs cell migration. Seminars in cell & developmental biology, 2009. Elsevier, 674-682.

ZHAO, M., BAI, H., WANG, E., FORRESTER, J. V. & MCCAIG, C. D. 2004. Electrical stimulation directly induces pre-angiogenic responses in vascular endothelial cells by signaling through VEGF receptors. *Journal of cell science,* 117**,** 397-405.

8. Declaration

I hereby declare that the submitted doctoral dissertation entitled: ‘Accelerating Skin Wound Healing *in vitro* - Establishment of an External Electrical Field System for Stimulating Keratinocytes ’ was written independently. I declare that all the results are from my research data, except for the quoted references and figures. Also, all the figures from the website or other papers have permission licenses. I am aware that false declarations or plagiarism would be punished, so I declare that these statements are true and have concealed nothing.

Place / Date / Signature：Tuebingen, 22.04.2022, Chao Lu

9. Acknowledgement

I never felt that I was so close to leaving until I started writing this part of my dissertation. Time flies and the first time I came to this beautiful country, the feeling of nervousness, excitement, and anticipation, everything seems to have happened yesterday. I have had a fantastic time over the past 3 years, and I know sometimes you will never know the value of a moment until it becomes a memory. Farewell is coming, and I would like to extend my thanks and appreciation to all those who offered me kind and professional help whenever I needed it.

First of all, I would like to express my sincere gratitude to my supervisor Prof. Jonas Kolbenschlag for his ongoing support and encouragement. I appreciate that he went out of his way to help me get integrated and offered his perspective and insights on my project. Without these helpful instructions, patience, and trust, I could not have accomplished the doctoral program. I am incredibly thankful for all that he has done.

I also want to thank Dr. Cosima Prahm, who offered great help to me while I was doing the project in Tuebingen. Her supervision and close follow-up ensured the smooth running of the project. It felt good to be working on a team with her to get the work done, and I appreciate everything she has taught me.

Special thanks to Prof. Andreas K. Nüssler, chief of the Siegfried Weller Institute. I am eternally grateful for his unselfish acceptance, excellent scientific support, and constructive suggestions on my project. It takes a special kind of person to dedicate effort and time to helping someone else navigate their study, so I feel lucky all the time. Special thanks to Dr. Sabrina Ehnert for her countless valuable pieces of advice. Her help was critical to getting the project done well and on time, and I learned a lot from her rigorous academic attitude and high professionalism.

Likewise, I am also grateful for all the support from my colleagues in the HPRV and SWI, who provided selfless theoretical and technical support for this project. The valuable advice and help they offered have dramatically ensured the project's smooth progress, and it is much appreciated.

Many thanks to my friends as well. I want to thank Yangmengfan Chen for spending absurd but maybe world-changing “philosopher's time” with me during lunch breaks. Thanks to Lu Fan and Qingjun Jiang for helping me out of

depression and urging me to complete the dissertation on time. Thanks to Michael Bressler for always sharing fantastic beer and happiness. Thanks to Chao Liu for setting an example for me to live a joyful, brave, and calm life, and I want to thank all my friends who entered my life. You helped me to understand the beauty and greatness of the world.

To my family members, I am sorry for leaving you so long, and a thousand thanks for supporting me all the time. Special thanks to my grandparents for their selfless love and care. I didn’t let you down and never will.

Most importantly, thank you, mom. I made it exactly as you expected. May your soul rest in peace.